(12)

SC5269.1FR

Copy No. 12

# NARROW-BAND WIDE FIELD-OF-VIEW FILTER STUDY

## FINAL REPORT FOR THE PERIOD
## July 7, 1980 through October 30, 1981



DARPA ORDER NO. 3650, AMENDMENT # 8
CONTRACT NO. N00014-80-C-0785

Prepared for

Defense Advanced Research Projects Agency
1400 Wilson Boulevard
Arlington, VA 22209

W.J. Gunning
Principal Investigator

MARCH 1982

Approved for public release: distribution unlimited

The views and conclusions contained in this document are those of the authors and should not be interpreted as necessarily representing the official policies, either expressed or implied, of the Defense Advanced Research Projects Agency or the U.S. Government.



Rockwell International
Science Center

UNCLASSIFIED

SECURITY CLASSIFICATION OF THIS PAGE (When Data Entered)

| REPORT DOCUMENTATION PAGE | | READ INSTRUCTIONS BEFORE COMPLETING FORM |
|---|---|---|
| 1. REPORT NUMBER | 2. GOVT ACCESSION NO. AD-A112 803 | 3. RECIPIENT'S CATALOG NUMBER |
| 4. TITLE (and Subtitle) NARROW-BAND WIDE FIELD-OF-VIEW FILTER STUDY | | 5. TYPE OF REPORT & PERIOD COVERED Final Report for the Period 07/07/80 through 10/30/81 |
| | | 6. PERFORMING ORG. REPORT NUMBER SC5269 1FR |
| 7. AUTHOR(s) W.J. Gunning | | 8. CONTRACT OR GRANT NUMBER(s) N00014-80-C-0785 |
| 9. PERFORMING ORGANIZATION NAME AND ADDRESS Rockwell International Science Center 1049 Camino Dos Rios Thousand Oaks, California 91360 | | 10. PROGRAM ELEMENT, PROJECT, TASK AREA & WORK UNIT NUMBERS NR 007-029 (240) DARPA Order No. 3650, Amendment #8 |
| 11. CONTROLLING OFFICE NAME AND ADDRESS Defense Advanced Research Projects Agency 1400 Wilson Boulevard Arlington, VA 22209 | | 12. REPORT DATE March 1982 |
| | | 13. NUMBER OF PAGES 88 |
| 14. MONITORING AGENCY NAME & ADDRESS(if different from Controlling Office) | | 15. SECURITY CLASS. (of this report) UNCLASSIFIED |
| | | 15a. DECLASSIFICATION/DOWNGRADING SCHEDULE |

16. DISTRIBUTION STATEMENT (of this Report)

Approved for public release; distribution unlimited.

17. DISTRIBUTION STATEMENT (of the abstract entered in Block 20, if different from Report)

18. SUPPLEMENTARY NOTES

19. KEY WORDS (Continue on reverse side if necessary and identify by block number)

20. ABSTRACT (Continue on reverse side if necessary and identify by block number)

With the advent of free space laser communications, and communication to submerged submarines in particular, the state-of-the-art in narrowband wide field-of-view spectral filters is being pushed to its limit. In the case of underwater communication, the combined effects of absorption and scattering result in a radiance function of large angular extent. Conventional narrow-band filters simply do not have suitably large angular fields-of-view to receive light from the full range of angles encountered. A shift of the

DD FORM 1 JAN 73 1473 EDITION OF 1 NOV 65 IS OBSOLETE

UNCLASSIFIED

SECURITY CLASSIFICATION OF THIS PAGE (When Data Entered)

transmission passband with angle of incidence leads to a decrease of signal transmission and proportionally larger background intensity. It was recently realized that a material modification of traditional birefringence interference filters, by using materials having large dispersion in birefringence near an isotropic point, could result in compact, narrowband filters having a dramatically increased field-of-view.

Under this contract the development of a dispersive birefringence filter was pursued both theoretically and experimentally. Because of near term programs to demonstrate a submarine laser receiver, the filter was designed to operate at $\lambda = 5320$ Å (doubled Nd:YAG) with a bandwidth of 1.8 Å and field-of-view of $\pm 60^{\circ}$ as measured in air. For this application, CdS was chosen for the dispersive birefringence elements. The design of the filter was that of a Lyot-Ohman birefringence filter in which the narrowband stages are modified to have enhanced fields-of-view. Such a filter has been substantially realized experimentally, and shows complete suppression of sidebands in the visible. Additional effort is required to fully demonstrate the extreme wide-field properties of the filter.

This study of birefringence filters at extremely large angles of incidence has stimulated additional work to study the effects of sheet polarizers and conventional waveplates under these conditions. Some of the effects discovered lead to unconventional conclusions regarding the design of polarization devices at large incident angles.

These developments in dispersive birefringence filters represent a major jump in the capabilities of narrowband spectral filters. Literature surveys and subsequent laboratory studies have led to the identification of potential dispersive birefringence materials which may extend the spectral range of operation to both shorter and longer wavelengths.

TABLE OF CONTENTS

LIST OF FIGURES

LIST OF FIGURES

LIST OF FIGURES

## REPORT SUMMARY

With the advent of free space laser communications, and communication to submerged submarines in particular, the state-of-the-art in narrowband wide field-of-view spectral filters is being pushed to its limit. In the case of underwater communication, the combined effects of absorption and scattering result in a radiance function of large angular extent. Conventional narrowband filters simply do not have suitably large angular fields-of-view to receive light from the full range of angles encountered. A shift of the transmission passband with angle of incidence leads to a decrease of signal transmission and proportionally larger background intensity. It was recently realized that a material modification of traditional birefringence interference filters, by using materials having large dispersion in birefringence near an isotropic point, could result in compact, narrowband filters having a dramatically increased field-of-view.

Under this contract the development of a dispersive birefringence filter was pursued both theoretically and experimentally. Because of near term programs to demonstrate a submarine laser receiver, the filter was designed to operate at $\lambda$ = 5320 A (doubled Nd:YAG) with a bandwidth of 1.8 A and field-of-view of $\pm 60°$ as measured in air. For this application, CdS was chosen for the dispersive birefringence elements. The design of the filter was that of a Lyot-Öhman birefringence filter in which the narrowband stages are modified to have enhanced fields-of-view. Such a filter has been substantially realized experimentally, and shows complete suppression of sidebands in the visible. Additional effort is required to fully demonstrate the extreme wide-field properties of the filter.

This study of birefringence filters at extremely large angles of incidence has stimulated additional work to study the effects of sheet polarizers and conventional waveplates under these conditions. Some of the effects discovered lead to unconventional conclusions regarding the design of polarization devices at large incident angles.

These developments in dispersive birefringence filters represent a major jump in the capabilities of narrowband spectral filters. Literature surveys and subsequent laboratory studies have lead to the identification of potential dispersive birefringence materials which may extend the spectral range of operation to both shorter and longer wavelengths.

# 1.0 INTRODUCTION

The development of a submarine laser communications system has resulted in specifications for a spectral filter which cannot be met by conventional approaches.[1-3] It is anticipated that in order to be most effective in gathering signal photons, the optical receiver should have an angular field-of-view (FOV) in sea water of ±40°. Because of the requirement of filtering to eliminate background, a narrowband (< 3 A) filter must be included. Unfortunately, no conventional filter can simultaneously meet these specifications because of a shift of the passband with angle-of-incidence. Fabry-Perot filters can easily meet the passband requirement but are severely limited in FOV.[4] Conventional thin film interference filters also suffer from FOV restrictions.[5] Birefringent filters made of quartz can achieve the required bandwidth but can only approach a FOV of ± 15° in water for a bandwidth of 3 A.[4] In addition, quartz birefringent filters of this bandwidth are quite large (~ 17 cm thick), requiring bulky optical collection systems. The FOV restriction of a standard birefringent filter may be accommodated by deconcentrating the light but at a sacrifice of collecting aperture for given filter size.

Recently several novel spectral filter designs were proposed and studied[6,7] including the dispersive birefringent filter[8-12] discussed here. This filter uses materials having large dispersion in the birefringence near an isotropic point[13-14] which results in simultaneously narrow bandwidth and large angular FOV. In addition the filter is compact and easily integrated into an optical collection system. The configurations of this filter may be any of those available for conventional birefringent filters,[15] however, because of its use at large angles of incidence, additional considerations may favor different configurations than are usually optimum for near normal incidence operation. The dispersive birefringent filter (DBF) has distinct advantages over several alternative approaches to wide FOV filters and such comparisons will be made in the main text of this report.

This device development program was actively pursued under IR&D support during intervals between periods of contract funding. In order to present a coherent discussion of the DBF development we will report here all results, whether obtained under IR&D or contract support.

# 2.0 THEORY

## 2.1 Birefringent Filters

Birefringent filters consist of linear sequences of birefringent elements and linear polarizers.[15,16] Many configurations are possible,[15] each having characteristic spectral properties and its own particular advantages and disadvantages. The simplest design, from the conceptual point of view, is that devised independently by Lyot[17] and Öhman.[18]

In Fig. 1, we present the structure of a Lyot-Öhman[19] filter. Each of the birefringent plates is oriented with its optic-axis in the plane of the plate and at 45° to the polarization direction of the polarizers. For a filter with N plates, the elements are in a thickness ratio of $1:2:4\cdots2^{N-1}$ with the thinnest plate being an integral number of full waves of phase retardation at the desired passband wavelength. Each of the N stages, consisting of one plate and two polarizers, has a transmission spectrum given by

$$\tau(\lambda) = \cos^2 \frac{\Gamma}{2} \quad , \tag{1}$$

where $\Gamma = 2\pi\Delta n\, d/\lambda$ is the phase retardation of the plate, $\Delta n$ is the birefringence, $n_e - n_o$, and d is the thickness of the plate. This channel spectrum is caused by the variation of $\Gamma$ with wavelength which causes the phase velocities of the two polarization modes to vary by different amounts at different wavelengths. Combining all N stages gives an overall transmission of

$$T = \frac{1}{4^N} \frac{\sin^2 (2^N \frac{\Gamma}{2})}{\sin^2 (\frac{\Gamma}{2})} \tag{2}$$

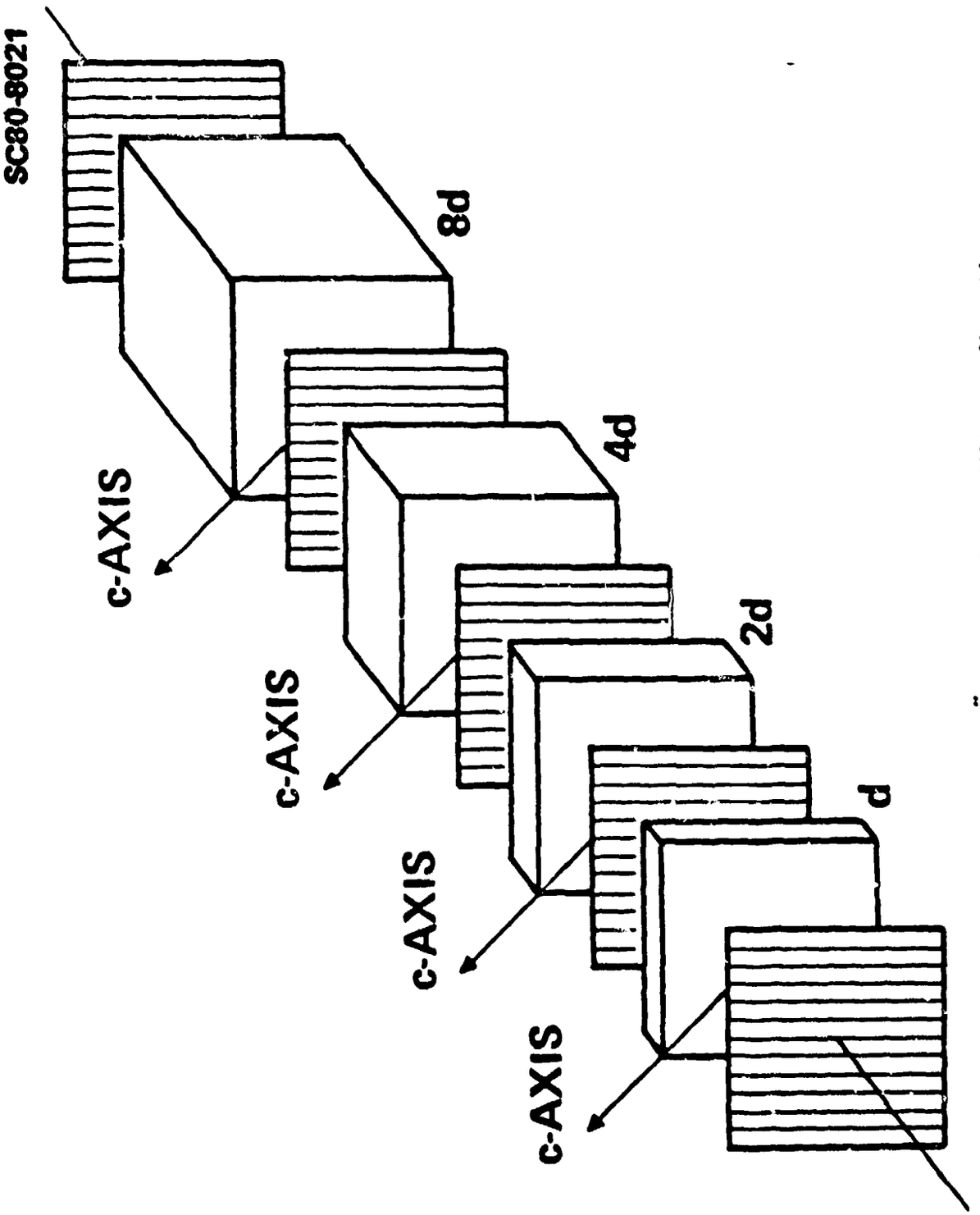


Fig. 1 Lyot-Öhman birefringent filter configuration.

In this expression, $\Gamma$ takes its value from the thinnest plate in the filter. The bandwidth, $\Delta\lambda_{1/2}$(FWHM), is determined by the thickest filter stage, while the free spectral range (FSR) is determined by the thinnest stage.

The parameter which determines the bandwidth of a filter is the differential phase retardation of the birefringent material employed.

$$\frac{d\Gamma}{d\lambda} = \frac{2\pi d}{\lambda}\left(\alpha - \frac{\Delta n}{\lambda}\right) \tag{3}$$

where $\alpha$ is the dispersion of the birefringence or

$$\alpha = \frac{d\Delta n}{d\lambda} \quad . \tag{4}$$

From Eq. (2) it is seen that the transmission spectrum is similar to that of a grating with $2^N$ lines. The bandwidth of the system is governed by that of the thickest plate and is given by

$$\Delta\lambda_{1/2} = 0.886\,\frac{2\pi}{2^N\left|\partial\Gamma/\partial\lambda\right|} = 0.886\,\frac{\lambda}{2^N\left|\alpha - \Delta n/\lambda\right| d} \tag{5}$$

where N is the number of stages and d is the thickness of the thinnest filter stage.

The free spectral range (FSR) of this filter (the wavelength internal between successive transmission bands) is determined by the bandwidth of the thinnest plate, and is given by

$$FSR = \frac{\lambda}{|\alpha - \Delta n/\lambda| d} \qquad (6)$$

Another structure, described by Solc,[20-22] makes use of many birefringent plates of identical thickness between a single pair of polarizers. The plates are oriented with their optic-axes rotated to prescribed angles to achieve the desired pass-band characteristics. Many additional variations exist between the two basic filter types,[15,16] the Lyot-Öhman and the Solc. In the rest of the discussion which follows, we will concentrate on the Lyot structure which is the configuration in which the first DFB has been constructed.

## 2.2 Dispersive Birefringent Filters

### 2.2.1 Effect of Dispersion on Spectral Properties

If we examine Eqs. (5) and (6) we see that the most basic properties of a Lyot-Öhman filter are determined by the differential phase retardation $d\Gamma/d\lambda = |\alpha - \Delta n/\lambda| d2\pi/\lambda$. For most birefringent materials from which filters have been constructed (quartz, calcite, KDP), the dominant contribution arises from the term $\Delta n/\lambda$, which varies rather slowly with wavelength. The effect of the dispersion term, $\alpha$, must indeed be taken into account, and can in some cases result in a 50% correction to the bandwidth of the filter.

Materials do exist, however, in which over some spectral range, the dispersion of the birefringence dominates the differential phase retardation.[13,14,23-25] This is most commonly observed in crystals which exhibit an isotropic (or iso-index) point where the birefringence vanishes. A partial list of these materials appears in Table 1.

Table 1

Dispersive Birefringent Materials and Their Spectral Regions of Strony Dispersion

| | |
|---|---|
| CdS | 5250 Å - 5500 Å |
| $Zn_xCd_{1-x}S$ | ~ 4000 Å - 5300 Å depending on x |
| $CdS_{1-x}Se_x$ | 5250 Å - 7100 Å depending on x |
| $AgGaS_2$ | $\lambda > 4970$ Å |
| $AgGa(S_xSe_{1-x})_2$ | 4970 Å - 8000 Å depending on x |
| $CdGa_2S_4$ | $\lambda > 4800$ Å |
| $MgF_2$ | uv |
| $Al_2O_3$ | uv |

For our filter development, we have chosen CdS since it is a stoichiometric crystal which is commercially available and has a large dispersion in the wavelength range of interest.[13] In Fig. 2, the birefringence of CdS is presented near its isotropic point. At $\lambda = 5320$ Å, the contributions to the differential phase retardation are

$$\frac{\Delta n}{\lambda} = 1.38 \times 10^{-6}\ \text{Å}^{-1} \tag{7}$$

and

$$\alpha = 0.7 \times 10^{-4}\ \text{Å}^{-1} \quad . \tag{8}$$

This is to be compared with quartz[26,27] whose small dispersion yields

$$\frac{\Delta n}{\lambda} = 1.8 \times 10^{-6}\ \text{Å}^{-1} \tag{9}$$

and

$$\alpha = -1.6 \times 10^{-7}\ \text{Å}^{-1} \quad . \tag{10}$$

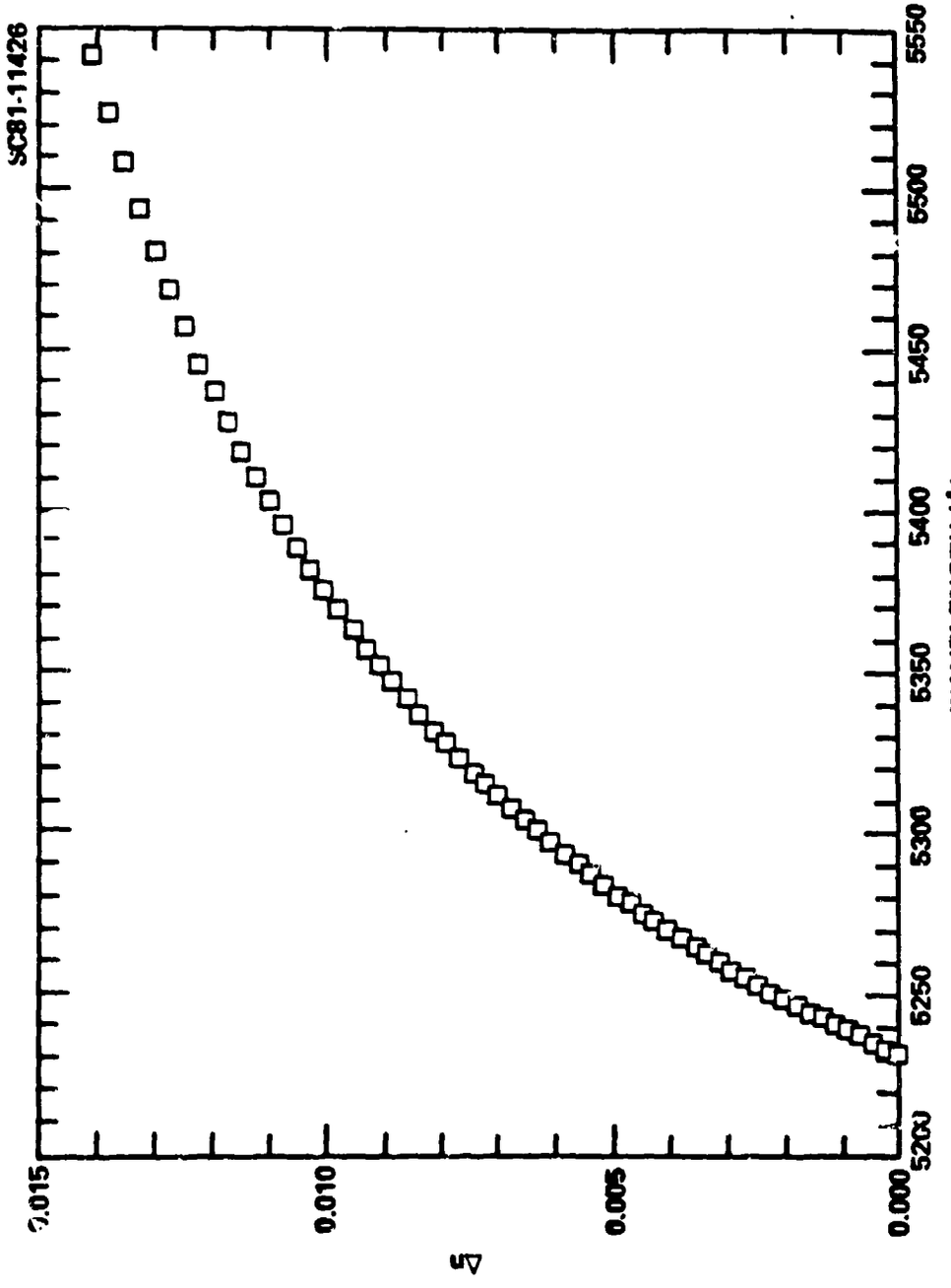


Fig. 2 Birefringence of CdS near the isotropic point.

The comparison of these two materials leads to dramatic conclusions. Because of the enhancement of $d\Gamma/d\lambda$ by the dispersion in CdS, much thinner crystal plates are required to produce a given bandwidth. The thickness reduction relative to a quartz filter at 5320 Å is by roughly a factor of 30. Therefore, the thickest plate of a Lyot-Öhman filter having bandwidth of 1.8 Å at 5320 Å (doubled Nd:YAG) would be 2.32 mm for CdS and 69 mm for quartz. This results in a great savings in filter volume, simplifying the optical collection system, and more than offsets the potential vignetting which would result from the limited crystal sizes which are available. Subangstrom bandwidths might be possible, if not for the absorption of the CdS, which is encountered because of the proximity of the operating wavelength to the absorption edge.[28] Operating at reduced temperature may partially alleviate this problem but a reduction in dispersion at $\lambda$ = 5320 Å is also observed.

An effect, which is also observed in the CdS filter, is the enhanced FSR which is possible. Since the dispersion of the birefringence decreases towards larger wavelengths, the bandwidths increase. This occurs at a much greater rate than is observed in "non-dispersive" materials. In a quartz filter the FSR increases by slightly more than a factor of two on the long wavelength side of the passband with the addition of each thinner stage. For CdS, the decreasing dispersion causes the FSR to increase much more rapidly which the addition of these blocking stages. As will be demonstrated later, this leads to total blocking of sidebands in the visible.

On the short wavelength side of the passband, the FSR increases by less than a factor of two per stage because of the increasing dispersion. However, the absorption of the CdS eliminates the shorter wavelength passbands resulting in a fully blocked filter.

### 2.2.2 Effect of Dispersion on the Field-of-View

Perhaps the most significant property of dispersive birefringent waveplates is their extremely large angular field-of-view. The phase retardation of a uniaxial plate of thickness d, with its optic-axis in the plane of the plate, is given by[19]

$$\Gamma = \frac{2\pi d}{\lambda}\left\{n_e\left(1 - \frac{a^2}{n_o^2} - \frac{b^2}{n_e^2}\right)^{1/2} - n_o\left(1 - \frac{a^2 + b^2}{n_o^2}\right)^{1/2}\right\} \qquad (11)$$

where $n_e$, $n_o$ are the extraordinary and ordinary refractive indices respectively and

$a = \sin\theta \sin\phi$

$b = \sin\theta \cos\phi$

$\theta$ = angle of incidence measured from plate normal

$\phi$ = azimuth angle measured between the plane of incidence and the optic-axis.

Near normal incidence this expression reduces to

$$\Gamma = \frac{2\pi\Delta n d}{\lambda}\left\{1 + \frac{\theta^2}{2n_o}\left(\frac{\cos^2\theta}{n_e} - \frac{\sin^2\phi}{n_o}\right)\right\} \qquad (12)$$

Inspection of this expression shows that, as $\theta$ increases, the phase retardation will increase, or decrease, from its normal incidence value, depending on the azimuth direction. This is caused by a combination of the increased optical path length and variation of the value of $n_e$ with direction of propagation in the crystal. If placed between parallel polarizers and illuminated by a focused monochromatic beam, the projected transmission will consist of a series of hyperbolic fringes. The field-of-view of the plate is defined to be that angle, $\theta_s$, at which $\Gamma$ has shifted by an amount large enough to shift the transmission peak by one half of its FWHM.

Expression (11) is valid for any birefringent material, whether it be dispersive or non-dispersive. It is this fact which leads to the greatly increased FOV of dispersive birefringence materials. A plate of CdS 2.32 mm thick will produce a 1.8 A bandwidth at $\lambda$ = 5320 A. However, the interference

order of the plate is only 32 full waves of retardation. If the dispersion were negligible, the bandwidth would be 104 A. The calculated FOV of this plate is ± 21°, which is what one would observe for any element having that constant value of Δn regardless of the dispersion. On the other hand, a nondispersive plate of the same Δn would require a thickness of 123 mm to produce a bandwidth of 1.8 A. In this case, the FOV would be only ±2.7.

Upon making a small angle approximation, and explicitly including the dispersion, the spectral shift may be calculated in both the dispersive and nondispersive regimes. One obtains[7]

$$\Delta\lambda = \frac{\Delta n}{2n^2|\alpha - \Delta n/\lambda|} \sin^2\theta\ (1-2\sin^2\phi) \tag{13}$$

At the FOV angle, the shift is equal to one half of one FWHM, and looking at the worst case azimuth angle where the shift is a maximum,

$$\sin\theta = \pm\, n\left|\frac{\Delta\lambda_{1/2}\ (\alpha - \Delta n/\lambda)}{\Delta n}\right|^{1/2} \tag{14}$$

This is only an approximation, and is not applicable for large incidence angles, but may be used for qualitative comparisons. For example, a 1.8 A CdS filter is predicted to have a FOV of ±21° while a quartz filter of similar bandwidth would have of FOV of only ±1.6°.

A further increase in the FOV can be achieved by using wide-field elements. The simplest manifestation is the Lyot-1 wide-field structure[19] shown in Fig. 3. The element is made of two birefringent plates of equal thickness and oriented with their axes crossed. A half-wave plate, oriented at 45°, is placed between the plates. In this way, the phase retardations of the two plates add, but spectral shifts, which are positive and negative in

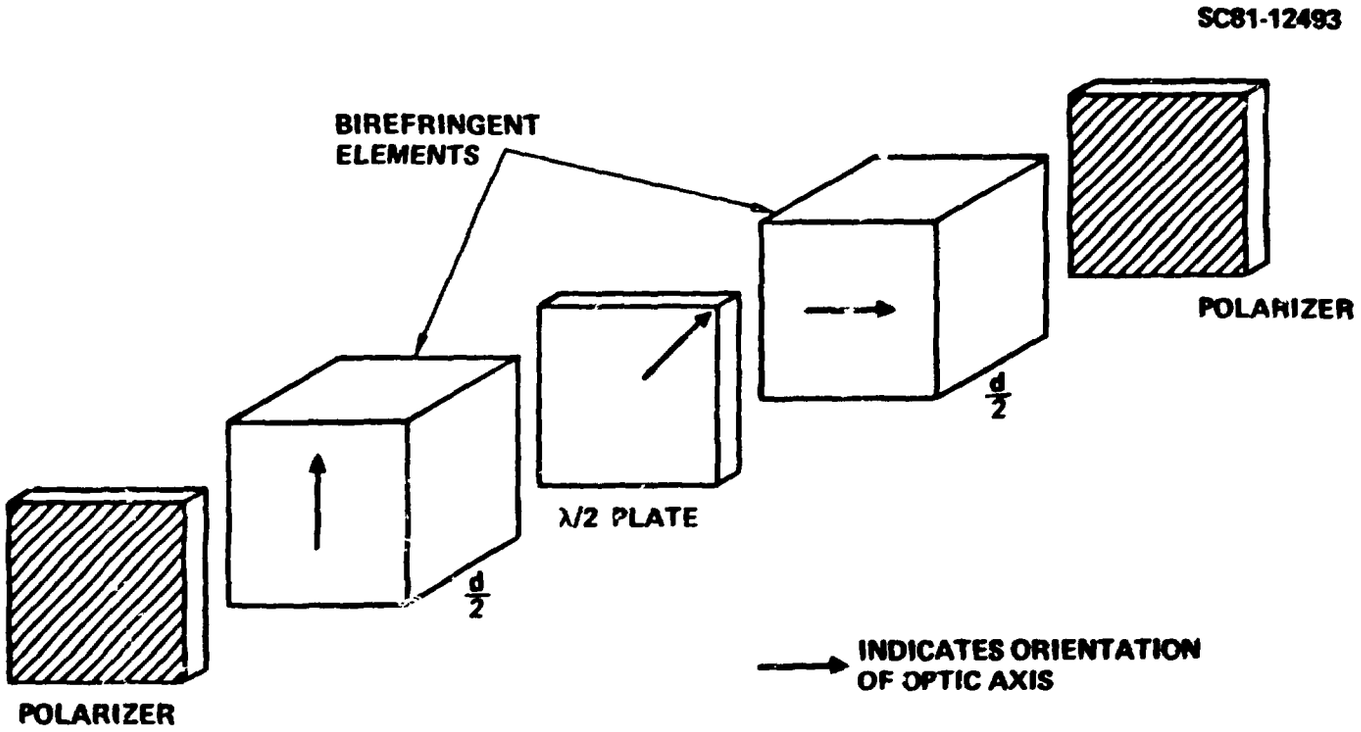


Fig. 3 Lyot-1 wide-field geometry.

adjacent quadrants, largely cancel each other. The monochromatic fringe pattern is now circular with a much larger radius than the hyperbolic pattern of a single plate. To describe the properties of a wide-field stage the phase retardation is written in the form

$$\Gamma_{WF} = 1/2\ [\Gamma(\theta,\phi) + \Gamma(\theta,\phi + \tfrac{\pi}{2})] \tag{15}$$

The field-of-view of a dispersive Lyot-1 element may be approximated by[8,9]

$$\sin\theta = \pm\, n\, \left|\frac{2n}{\Delta n}\right|^{1/2} \left|\frac{\Delta\lambda_{1/2}|\alpha - \Delta n/\lambda|}{\Delta n}\right|^{1/2} \tag{16}$$

This expression is found to lead to significant errors at the large angles encountered since small angle approximations have been made. However, the additional factor of $|2n/\Delta n|^{1/2}$ indicates the significant increase in FOV which is realized by this structure. To obtain accurate predictions of the FOV of various filters in their wide-field configurations, calculations are required of the bandpass properties of each filter at various angles of incidence, using the exact expression of Eq. (11) for the phase retardation. One finds that the FOV of a 3 A bandwidth Lyot-1 quartz filter is ± 20° while the FOV of a 1.8 A CdS filter at λ = 5320 A is so large that its practical limit is determined by the wide-field properties of the polarizers and waveplates. The calculated spectral shift at an angle of incidence of 60° in water is only 0.25 A. Therefore, in its field-widened configuration, a CdS filter will easily accept light from the entire radiance cone anticipated in underwater scenarios.

Other wide-field filters have been studied recently for use in undersea laser communications. The electro-optic coupled-wave filter[7] operates at the iso-index wavelength of the $AgGaS_2$ filter material. Its

field-of-view has been found to be limited by the optical rotation which has a pronounced effect at this wavelength. However, the more severe restriction results from its fixed wavelength of operation. It is necessary to tailor the material composition to match the available laser wavelength. This is also a problem for atomic resonance filters,[6] in which a material must be selected whose optical transitions exactly match the laser wavelength. This is not as significant an issue for the dispersive birefringent filter since it does not depend on the point spectral properties of the optical material. The passband can be selected by simply fabricating the birefringent plates to the required thickness, provided the laser wavelength lies within the materials' range of large birefringence dispersion which typically covers a few hundred angstroms.

## 3.0 EXPERIMENTAL DEVELOPMENT

The results presented below have been reported in the literature[10] and at several professional conferences.[11,12]

### 3.1 Verification of Physical Principles

In the discussion of the theory of dispersive birefringence filters, definite predictions were made regarding their spectral and angular properties. Simple experiments were performed to verify each of these predictions.

Figure 4 is a plot of the polarization interference spectrum of a single filter stage. The CdS plate is 1.16 mm thick which makes it a 16th-order stage at $\lambda$ = 5320 A. Measurements of the transmission were made in a single beam experiment which partially accounts for the variation of the intensities of the transmission maxima. The peak at $\lambda$ = 5320 A is found to have a FWHM of roughly 4 A with peak widths increasing towards longer wavelengths because of the decreased dispersion. In comparison, a quartz element of similar bandwidth at $\lambda$ = 5320 A would be 40 mm in thickness. Consequently a great reduction in filter thickness is realized in regions of large birefringence dispersion.

The most important prediction relating to the angular properties was also verified. Spectral scans were made of a single filter stage at various angles of incidence near $\lambda$ = 5300 A. As we have shown earlier, by Eq. (11), the angle induced shift vanishes in two nearly orthogonal planes of incidence, while the shift is a maximum in planes which bisect these special directions. In these measurements, the birefringent plates were rotated about an axis which produced the largest spectral shift. The CdS sample has a FWHM of 4.2 A at the measurement wavelength. For comparison, a $TeO_2$ crystal of similar bandwidth was measured. Figure 5 shows the measured spectral shift in terms of percentage of one FWHM for various angles of incidence. The comparison is striking. For CdS at 20°, a shift of 20.7% of one FWHM is predicted

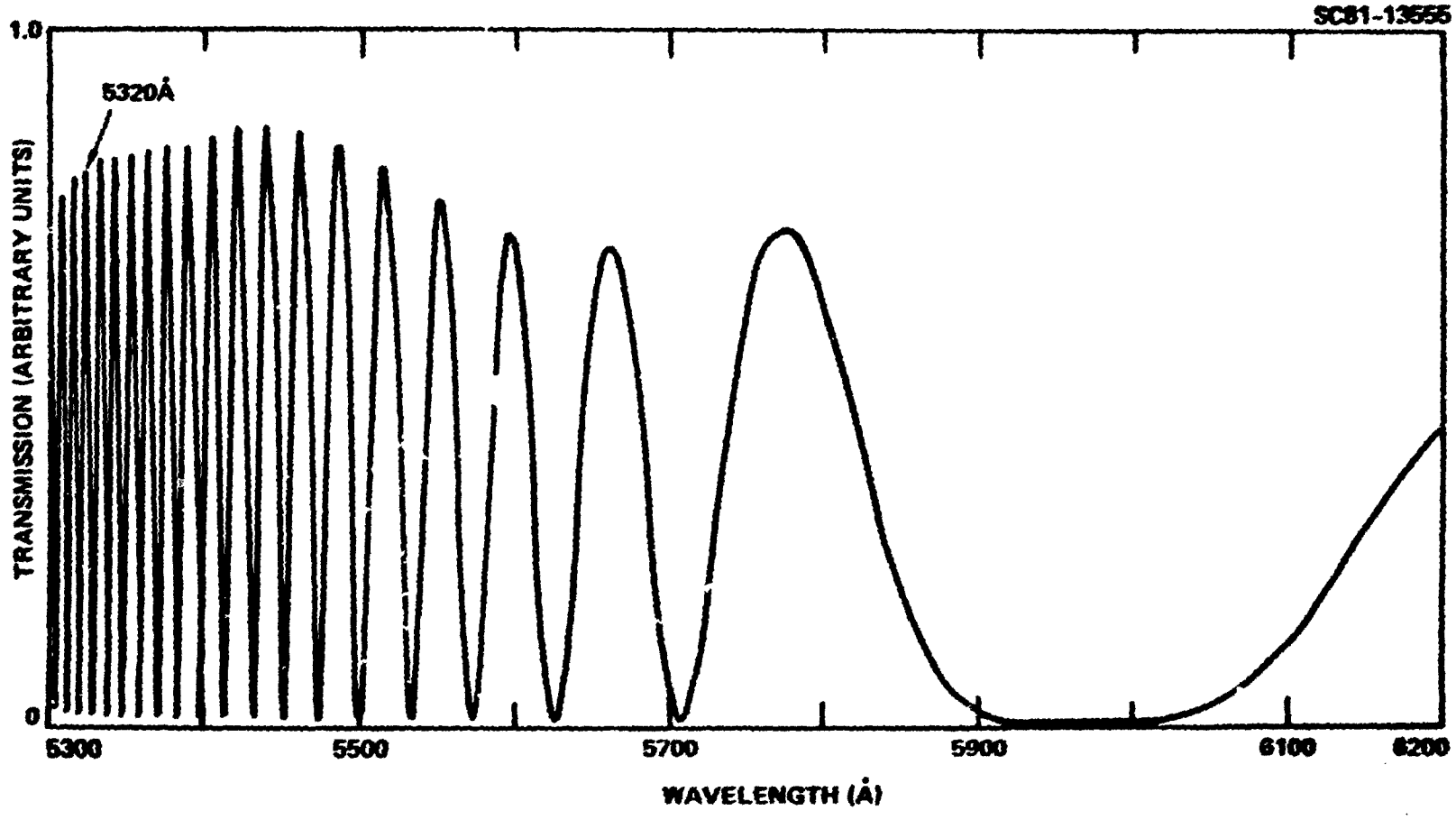


Fig. 4 Polarization interference spectrum of a 16th-order CdS filter stage.

SC80-10432

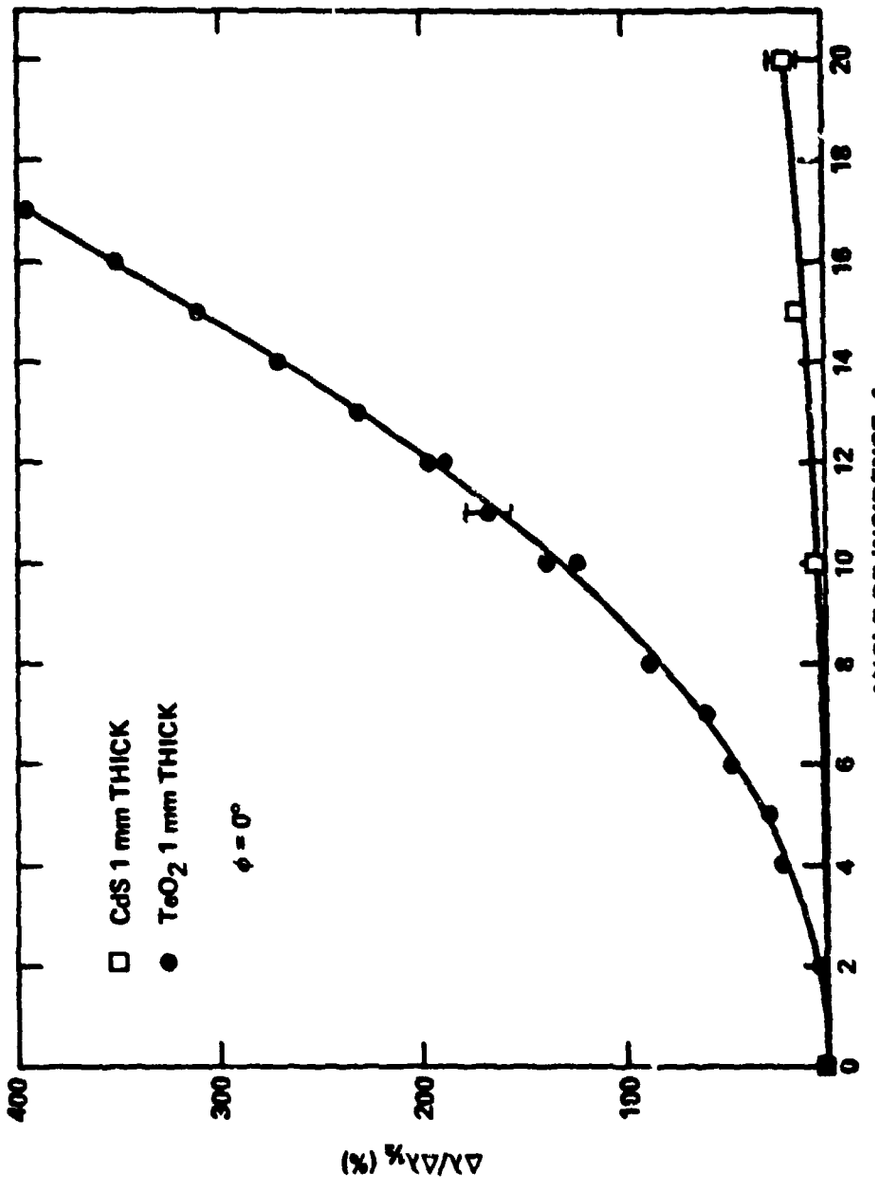


Fig. 5 Measured spectral shift vs angle of incidence for CdS and $TeO_2$.

and in excellent agreement with the observed value of 19.5%. The calculated FOV of this plate is 33°. The results for $TeO_2$, which can be simply related to that expected for quartz by the ratio of their refractive indices, indicate a FOV of only 6.1° corresponding to a shift of 50% of the bandwidth, $\Delta\lambda_{1/2}$.

With the above results, we can proceed to the problem of constructing a complete DBF filter using CdS. In the following sections we will discuss the relevant optical properties of CdS, the design and modeling of the filter and various experimental tests of the filter and its individual components.

## 3.2 Material Properties and Filter Design and Modeling

Cadmium sulfide has been chosen as a prototype material for DBF development because of its commercial availability and its large birefringence dispersion at $\lambda$ = 5320 A.[13] Its solid state properties have been the subject of extensive study and many interesting physical phenomena have been observed.[29] The occurrence of an iso-index crossing outside of the region of strongest absorption is presently thought to arise from an anisotropic spin-orbit splitting of the conduction band as observed in the reflectance spectrum.[30] In the usual case of an anisotropic band structure, the index crossing occurs at shorter wavelengths, near the peak of the absorption resonance. This anomalous occurrence of the isotropic point in a region of low loss in CdS, and several other materials, leads to the large dispersion in the birefringence. CdS also exhibits a wide range of optical phenomena associated with exciton levels in the band gap.[31,32] These can be quite sample dependent, changing dramatically with impurity type and growth condition. The roles that these phenomena play in affecting the optical properties and bulk absorption at $\lambda$ = 5320 A are not yet entirely understood.

To adequately model a CdS DBF filter, accurate knowledge of its optical properties is imperative. The birefringence of CdS was measured by a simple polarization interference measurement. A single Lyot-type stage was constructed using a crystal whose thickness was accurately determined. Spectra were recorded using a SPEX double monochrometer with subangstrom

resolution. Maxima occur when the condition

$$\frac{\Gamma}{2} = m\pi \tag{17}$$

is met where m is an integer. To determine the correct interference order, a degenerate mode coupling measurement was performed.[33] This procedure, which uniquely determines the isotropic point, consists of measuring the transmission of the plate between crossed polarizers with its optic-axis parallel to a polarizer axis. Where the birefringence is finite, no light is transmitted. However, at the isotropic point, where the ordinary and extraordinary modes are degenerate, residual internal strains are sufficient to induce coupling and lead to a peak in the transmission spectrum (see Fig. 6). Once identified, the iso-index wavelength determines the zeroth order peak in the interference spectrum and each order may then be identified unambiguously. Figure 2, shown earlier, presents the measured birefringence of CdS.

The birefringence data were fit to the empirical function,

$$\Delta n = \log_{10}(A_0 + A_1\lambda + A_2\lambda^2 + A_3\lambda^3) \tag{18}$$

with

$$A_0 = -0.175193 \times 10^3$$
$$A_1 = -0.962987 \times 10^{-1}$$
$$A_2 = -0.17550 \times 10^{-4}$$
$$A_3 = 0.106671 \times 10^{-8}$$

This expression has no real physical significance but does provide a good fit to the data in the wavelength range, 5235 A $< \lambda <$ 5500 A, with a minimum of fitting parameters.

In order to calculate the phase retardation exactly, the values of the individual indices are required as well as the birefringence. Values for

SC82-16322

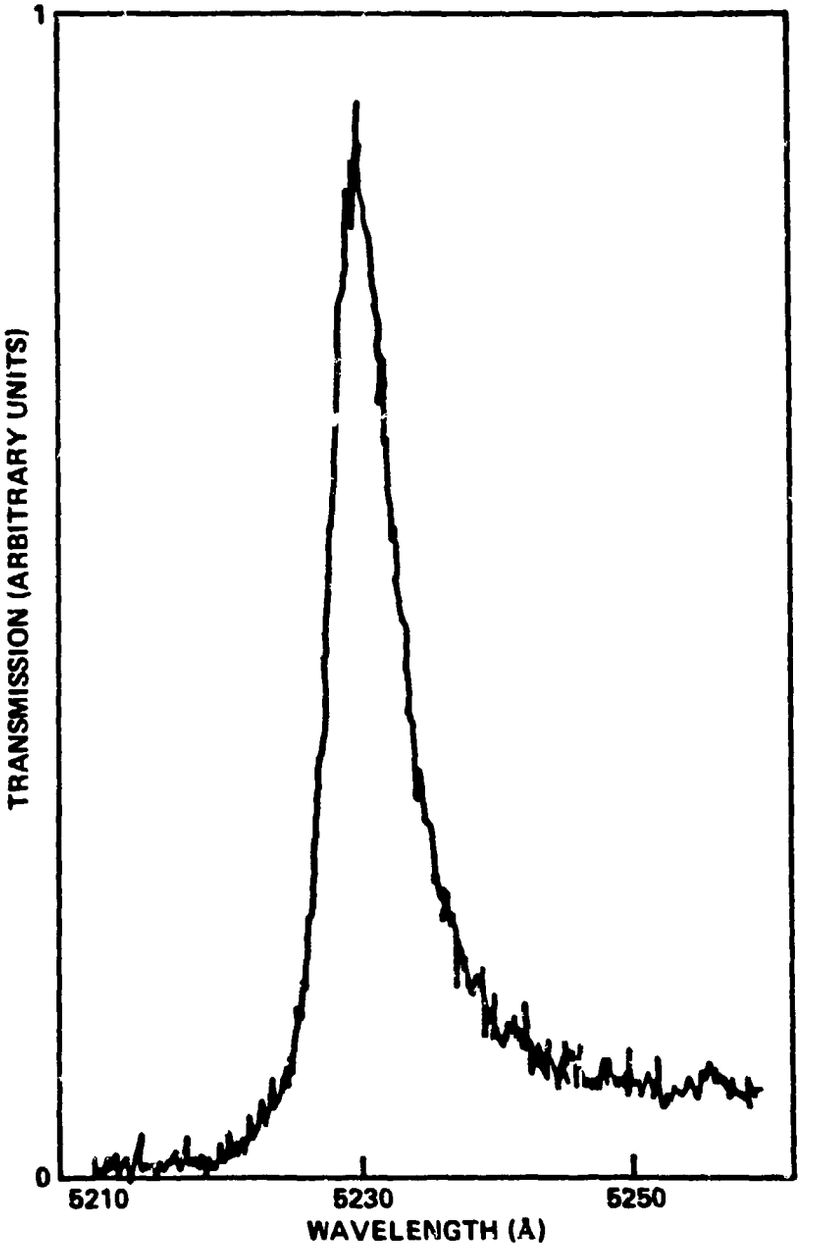


Fig. 6 Measurement of iso-index mode coupling response.

$n_o$ were taken from the literature[34] and were numerically fit to a Sellmeir equation of the form

$$n_o^2 = 1 + \frac{A_1\lambda^2}{\lambda^2 - A_3^2} + \frac{A_2\lambda^2}{\lambda^2 - A_4^2} \tag{19}$$

with parameters

$$A_1 = 0.38038$$
$$A_2 = 0.42397 \times 10^1$$
$$A_3 = 0.47 \times 10^4$$
$$A_4 = 25 \quad .$$

The extraordinary index can then be calculated, point by point, by the relationship $\Delta n = n_e - n_o$ using the above expressions for $\Delta n$ and $n_o$.

Since the operating wavelength, $\lambda_o$ = 5320 A, lies near the CdS band edge, it is important to include the bulk absorption and other loss mechanisms in the filter model. The CdS losses, which are anisotropic at the band edge, are incorporated by reworking the single filter stage problem in which each polarization experiences a different absorption coefficient which is considered to be wavelength dependent. Absorption data were obtained from the work of Thomas, et al,[28] and fit to the equation

$$\alpha = 10^{(A_0 + A_1\lambda + A_2\lambda^2)} \tag{20}$$

| $\alpha_\parallel$ (cm$^{-1}$) | $\alpha_\perp$ (cm$^{-1}$) |
|---|---|
| $A_0 = 0.8405684 \times 10^3$ | $A_0 = 0.4551128 \times 10^3$ |
| $A_1 = -0.3069106$ | $A_1 = -0.1576986$ |
| $A_2 = 02798109 \times 10^{-4}$ | $A_2 = 0.1356423 \times 10^{-4}$ |

With the above expressions for the refractive indices and absorption coefficients, most of the properties of a CdS DBF can be rather accurately predicted.

An additional practical material property is the temperature dependence of the birefringence or, more directly, the temperature dependenc of the bandpass position. Measurements of the spectral shift vs temperature of a single stage interference spectrum were made near room temperature. Results are shown in Fig. 7 as positions of interference minima vs temperature. The temperature coefficient at room temperature for $\lambda \approx 5300$ Å is found to be 0.7 Å/K. This value is to be compared with quartz whose temperature coefficient is ~ 0.56 Å/K[17] and that of conventional thin film interference filters which is roughly 0.3 Å/K.[35]

Using the relationships for the optical properties of CdS described above, a model could be constructed for calculating filter properties. Because of the dichroism present at the absorption edge, it was necessary to write the expression for single stage transmission in the form

$$\tau_i = \frac{1}{4}\left( e^{-\alpha_\parallel d_i} + e^{-\alpha_\perp d_i} + 2e^{-\frac{d_i}{2}(\alpha_\parallel + \alpha_\perp)} \cos\Gamma(\theta,\phi) \right) \tag{21}$$

where $\Gamma(\theta,\phi)$ is given by Eqs. (11) or (15) for Lyot or Lyot-1 stages respectively. This reduces to $\tau_i = e^{-\alpha d_i} \cos^2 \frac{\Gamma}{2}$ when $\alpha_\parallel = \alpha$ as expected. Assuming a Lyot-Öhman filter of N stages, the transmission becomes

$$T = A \prod_{i=1}^{N} 0.25\left( e^{-\alpha_\parallel d_i} + e^{-\alpha_\perp d_i} + 2e^{-\frac{d_i}{2}(\alpha_\parallel + \alpha_\perp)} \cos\Gamma_i \right) \tag{22}$$

where A is a constant which includes the effect of polarizer absorption and other possible losses. If all interfaces are antireflection coated and

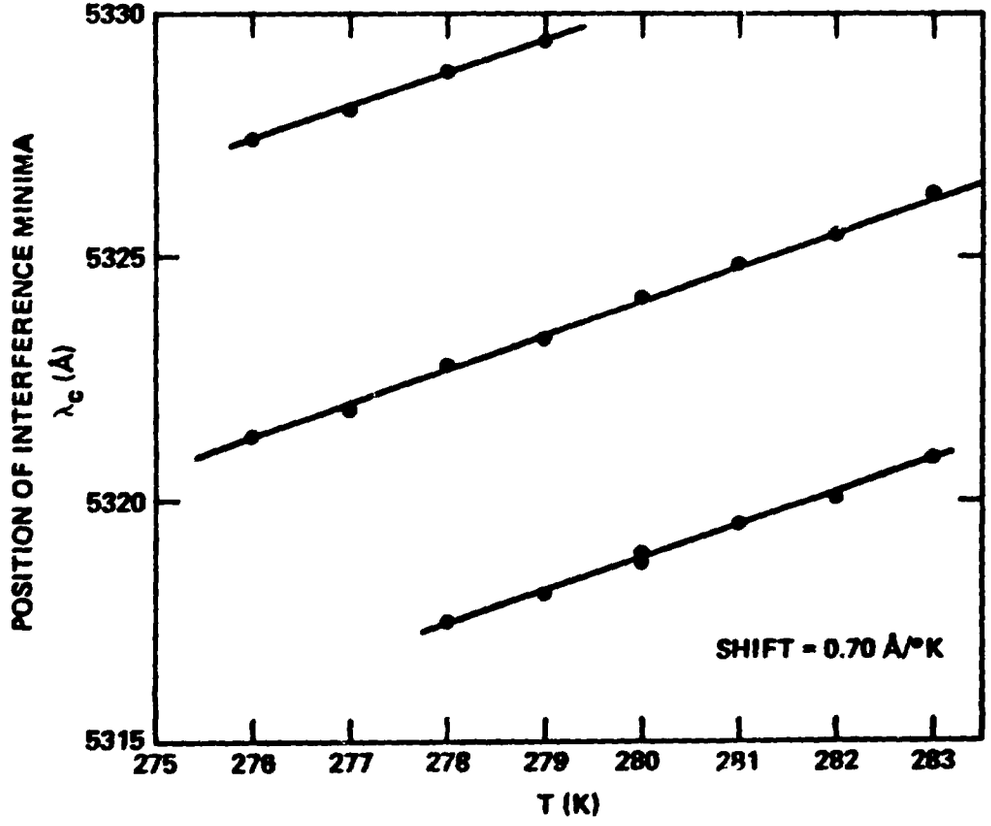


Fig. 7 Temperature dependence of CdS interference minima.

scatter free, then A is determined solely by polarizer losses in the form $A = 0.5\ (t)^{N+1}$, where t is the internal transmission of a single polarizer in polarized light.

Additional effects might be included in the exact filter model but at present are not well enough understood to allow their inclusion. For example, the degradation of polarizer properties for off-axis rays is well known and contributes to increased out-of-band transmission.[37] However, complete understanding of this effect is not yet available, making inclusion into the model difficult.

Other effects not included, are the field-of-view properties and achromaticity of the half-wave plates used in the Lyot-1 stages. These effects may be included, but would, at this time, require a reformulation of the model. With the above exceptions, the model presented here may be used to model a CdS Lyot-type DBF rather accurately. The additional data required are simply the plate thicknesses and assignment of Lyot-1 stages. During the course of the filter design, it was discovered that the free spectral range of the filter could be greatly increased by adding one additional half-integral order CdS waveplate between crossed polarizers. To accommodate this type of stage, the only modification is a change of sign of the $\cos\Gamma(\theta,\phi)$ term in Eq. (21).

In designing a filter for a specific wavelength, the Lyot-Öhman structure allows a discrete set of bandwidths. The simplest sequence begins with a first-order stage (i.e., having its first interference maximum beyond the iso-index point at the passband wavelength). Each additional Lyot stage reduces the bandwidth by a factor of two. Other sequences, beginning with odd-order stages (3:6:12:24....for example), lead to additional bandwidth possibilities. However such configurations limit the FSR which can be achieved.

The bandwidths which might be realized in a traditional birefringent filter form nearly a continuum since relatively high order plates are employed, and a wider array to interference order sequences may be used.

Calculations were performed for a four-stage 3:6:12:24-order filter, which was the original DBF design. An example of this calculation is shown in the following section for comparison with measured spectra. The inclusion of the CdS absorption qualitatively predicts the intensity variation between the various transmission maxima.

The final design chosen, was a seven-stage filter with order sequence 1:1.5:2:4:8:16:32. This is expected to have a bandwidth of 1.8 A, and the use of the 1.5-order stage is expected to eliminate the last residual sidebands in the visible spectrum. Assuming peak transmission of the polarizers of 95%, the calculated filter transmission is 22% in unpolarized light. Three or four of the high order stages may be field-widened to increase the FOV to best match the radiance function encountered under various situations. The calculated transmission of this filter, in the wavelength internal 5200 A < $\lambda$ < 5500 A, is shown in Fig. 8. Sidebands which are present near 5450 A are an artifact of the empirical fit of the birefringence data and are not expected to be present in the actual filter.

## 3.3 Demonstration of a Dispersive Birefringent Filter

The initial demonstration of the DBF was based on a four-stage Lyot-Öhman design with plates having the interference order sequence of 3:6:12:24. These plates were purchased from, and fabricated by, Cleveland Crystals, Inc. An attempt was made to fabricate each plate to a specified physical thickness. A photograph of the elements of this filter is shown in Fig. 9. The two thinner plates remain fixed to their polishing backing plates for support. (We have since demonstrated that plates as thin as fourth-order can be easily handled unsupported.) Figure 10 is a computer generated spectrum of this four-stage design while the measured spectrum appears in Fig. 11. Qualitatively, the measured spectrum is in excellent agreement with the calculated response. The change in relative peak intensities is caused by the proximity of the CdS absorption edge. Additional sidebands occur in the measured spectrum which were found to result from a thickness error in two of

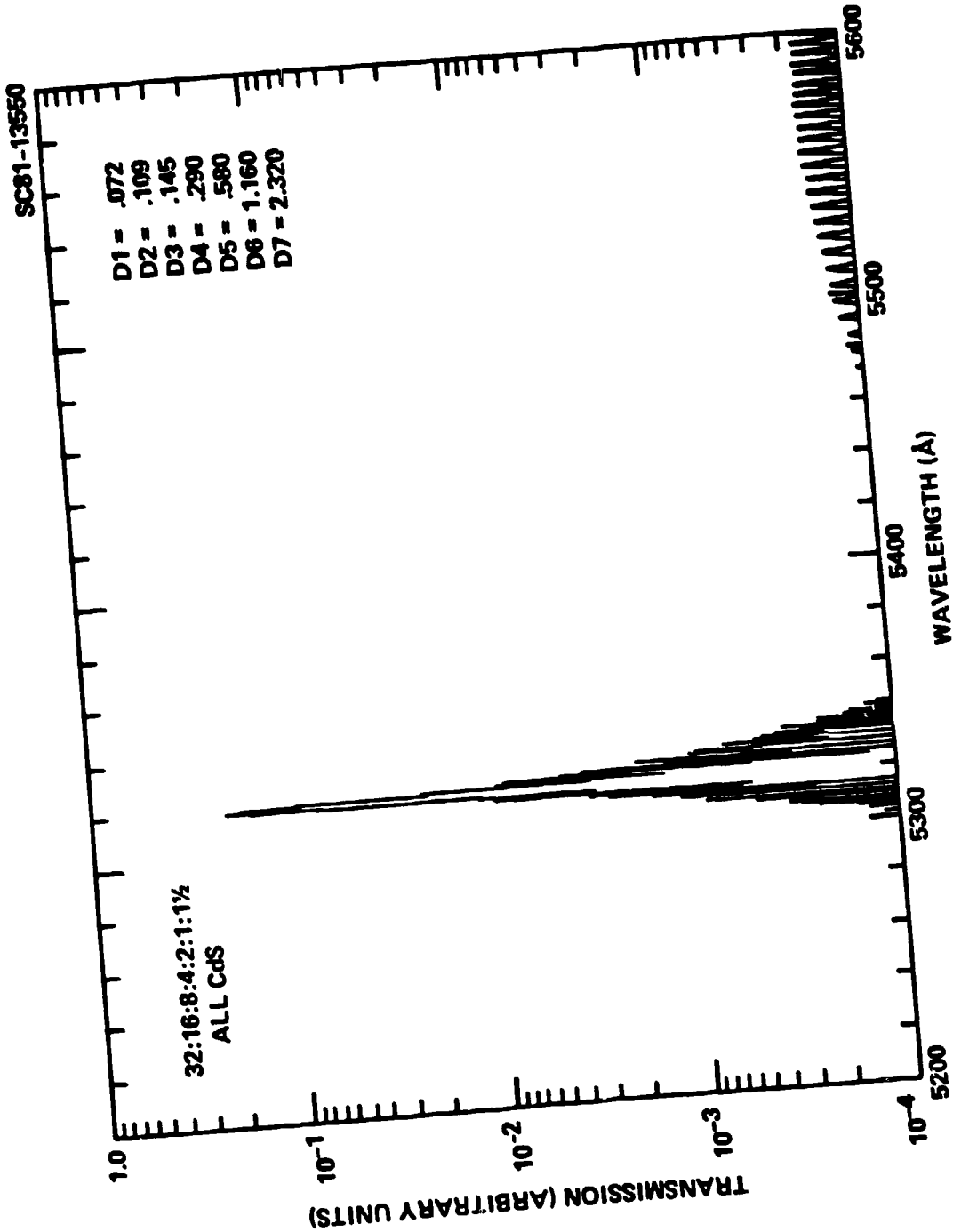


Fig. 8 Calculated transmission of a seven-stage CdS filter.

SC81-15422

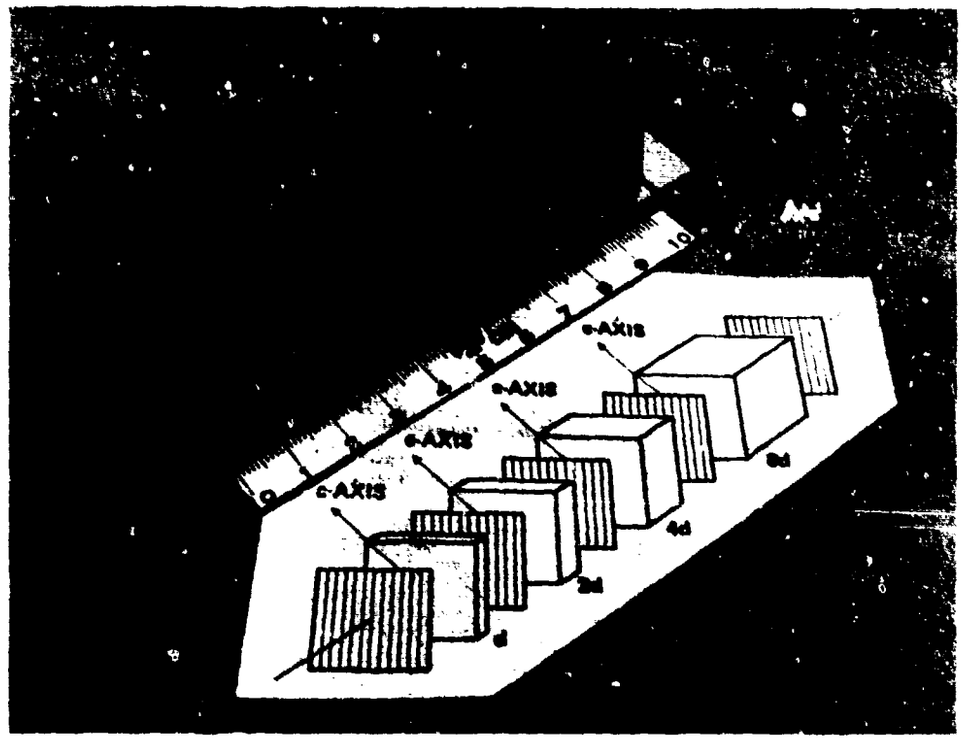


Fig. 9 Four-stage DBF filter elements.

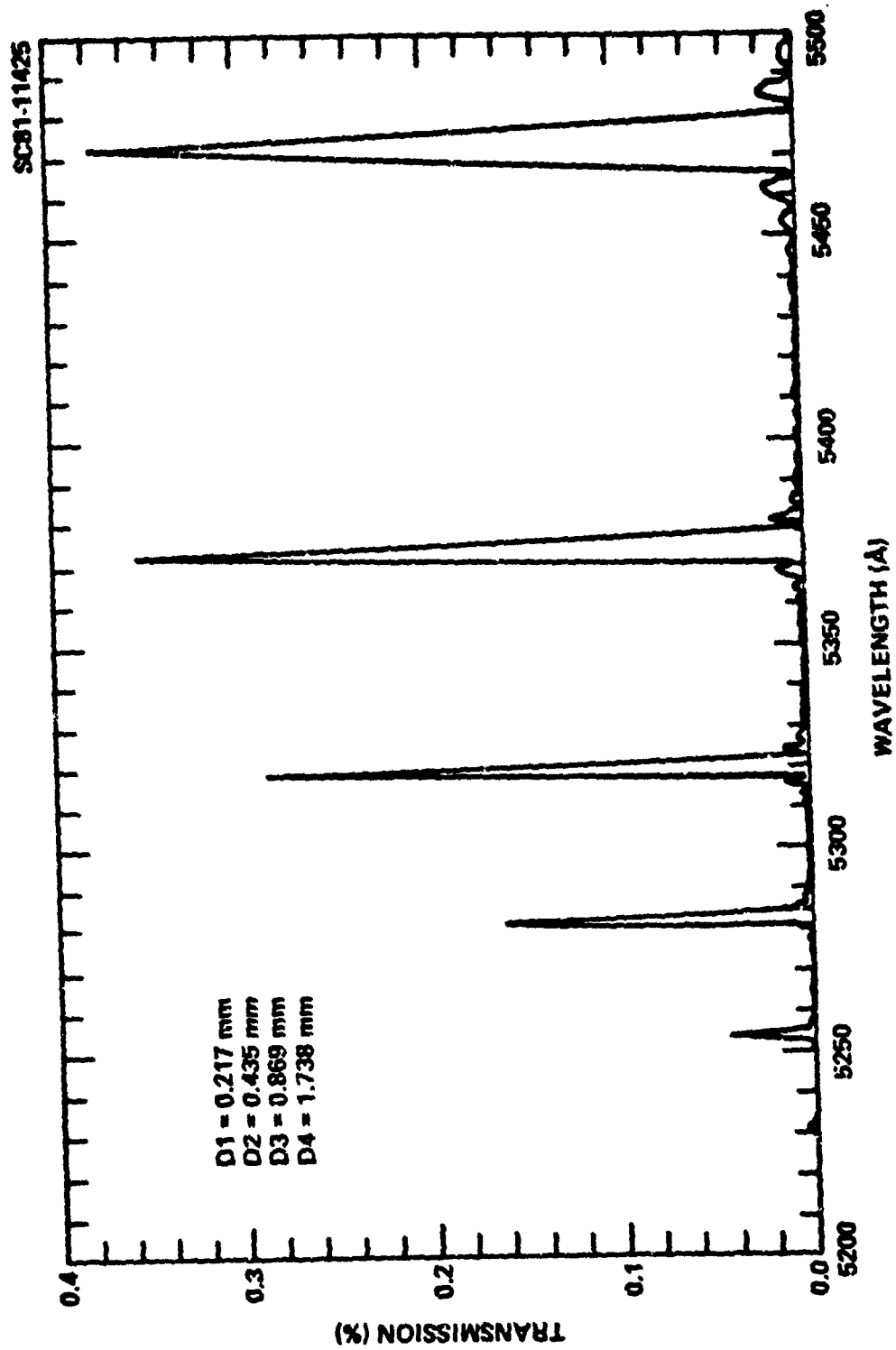


Fig. 10 Calculated spectrum of four-stage CdS filter.

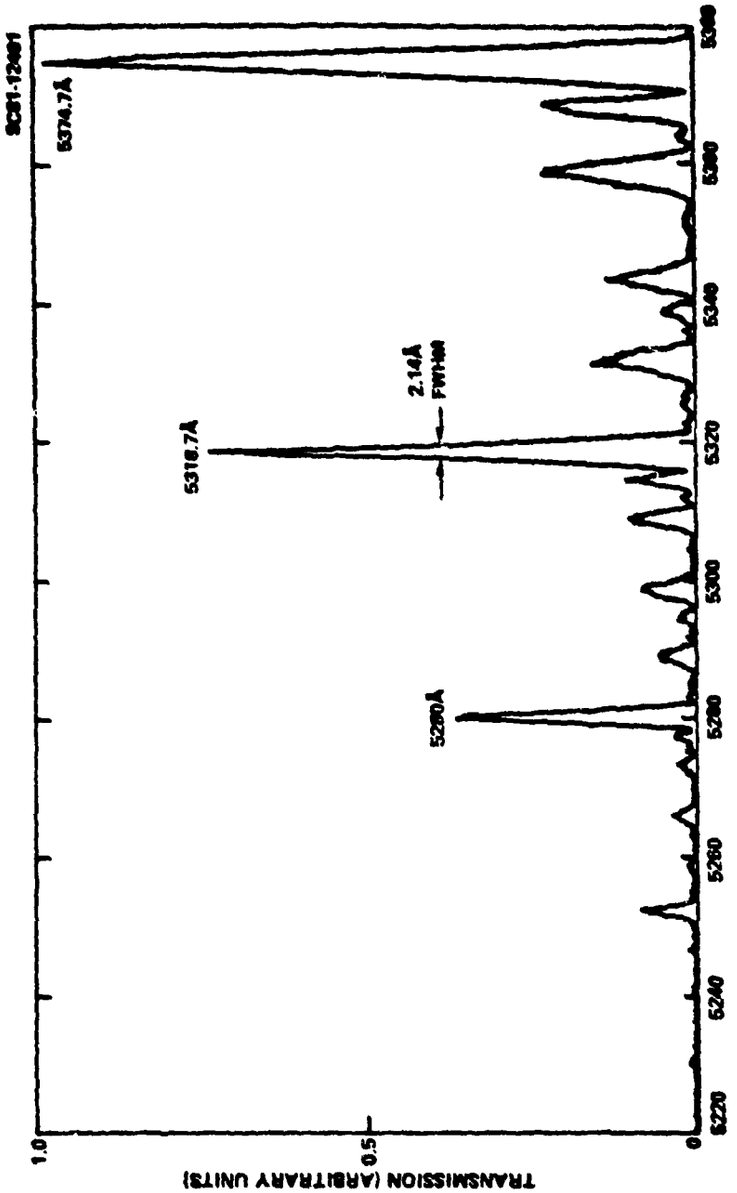


Fig. 11 Measured spectrum of four-stage CdS filter.

the plates. The difficulty in fabricating plates to a specified physical thickness was resolved by fabricating plates to the desired phase retardation thickness, as described below. However, these results verified the validity of the filter model, and provided the necessary experience for the fabrication of the seven-stage filter modeled above.

For the seven-stage filter, single crystal plates of high resistivity optical quality CdS were obtained from Cleveland Crystals, Inc. One inch square plates, of various thicknesses were fabricated with the C-axis oriented in the plane and parallel to an edge. In order to accurately determine the optical thickness of each plate during fabrication, a modification was made in the polishing apparatus which permitted periodic optical monitoring of the polarization interference spectrum. This was done since the required thickness tolerances make fabrication to a specified physical thickness very difficult as described above. Therefore, each plate was mounted on a Pyrex substrate in such a way that the entire polishing jig could be mounted in the optical test apparatus. By measuring the interference spectrum of the plate between parallel polarizers it was possible to fabricate each plate to the required order of interference. During the measurement, a surface thermometer monitored the temperature of the crystal so that corrections could be made to the transmission spectrum. Consequently, each plate was fabricated to the correct order at the specified operating temperature. The thinner plates in the filter (0.145 mm and less) were cemented to thin glass plates for support.

Several of the CdS plates were index matched to the lower index materials in the filter structure. This is required because the high index of the CdS and the many interfaces in the filter. However, problems with the coating equipment prevented optimum index matching of all of the elements in the filter. An upgraded deposition system is being prepared for further filter development work.

The polarizers used in the filter are Polaroid HN-38 material. MEK and methyl cellosolve were used to strip off the cellulose acetate butyrate backing material. The resulting thin PVA polarizer material was cemented

between thin glass cover slips. This procedure was employed to reduce the scatter of the polarizers[36] and to provide a more rigid, planar structure. HN-38 material was chosen because of its high extinction efficiency, but as a result, also represents a major loss mechanism in the filter. Procedures were developed for increasing the transmission of the polarizers without severely degrading their extinction properties. This will be discussed in more detail later.

For the measurements reported below, simple Lyot-Öhman stages were assembled. Results on wide-field stages are described later. In Fig. 12 the individual filter stage transmission spectra are presented for all but the 32nd-order stage (which was built up from two 16th-order plates). The broad structures, present at long wavelengths for even the thickest plates, promise to produce a very large free spectral range.

In assembling the filter elements, a silicon elastomer was used to "grease" the plates together. The material has high optical transmission and the high viscosity provides support for the elements while allowing for alignment adjustment and ease of disassembly. Figure 13 shows the transmission spectrum of the filter as additional thinner stages are added, again beginning with a 16th-order stage.

The complete seven-stage filter is shown in an edge on view in Fig. 14. A substantial percentage of the total thickness is due to the glass support plates which were required for the three thinnest stages. It is anticipated that the thickness of these plates can be substantially reduced, if not entirely eliminated, by bonding the thin crystal plates to polarizer elements. Figure 15 shows the transmission spectrum of this seven-stage filter with the full aperture illuminated in collimated light. As expected, no sideband structure is evident at shorter wavelengths because of the CdS absorption.[28] At longer wavelengths, a few small sidebands are found, which are probably the result of a slight thickness error found in one of the plates. Spectral scans from 4000 A and 8000 A further demonstrated the complete blocking of the filter in the visible (see Fig. 16). The measured

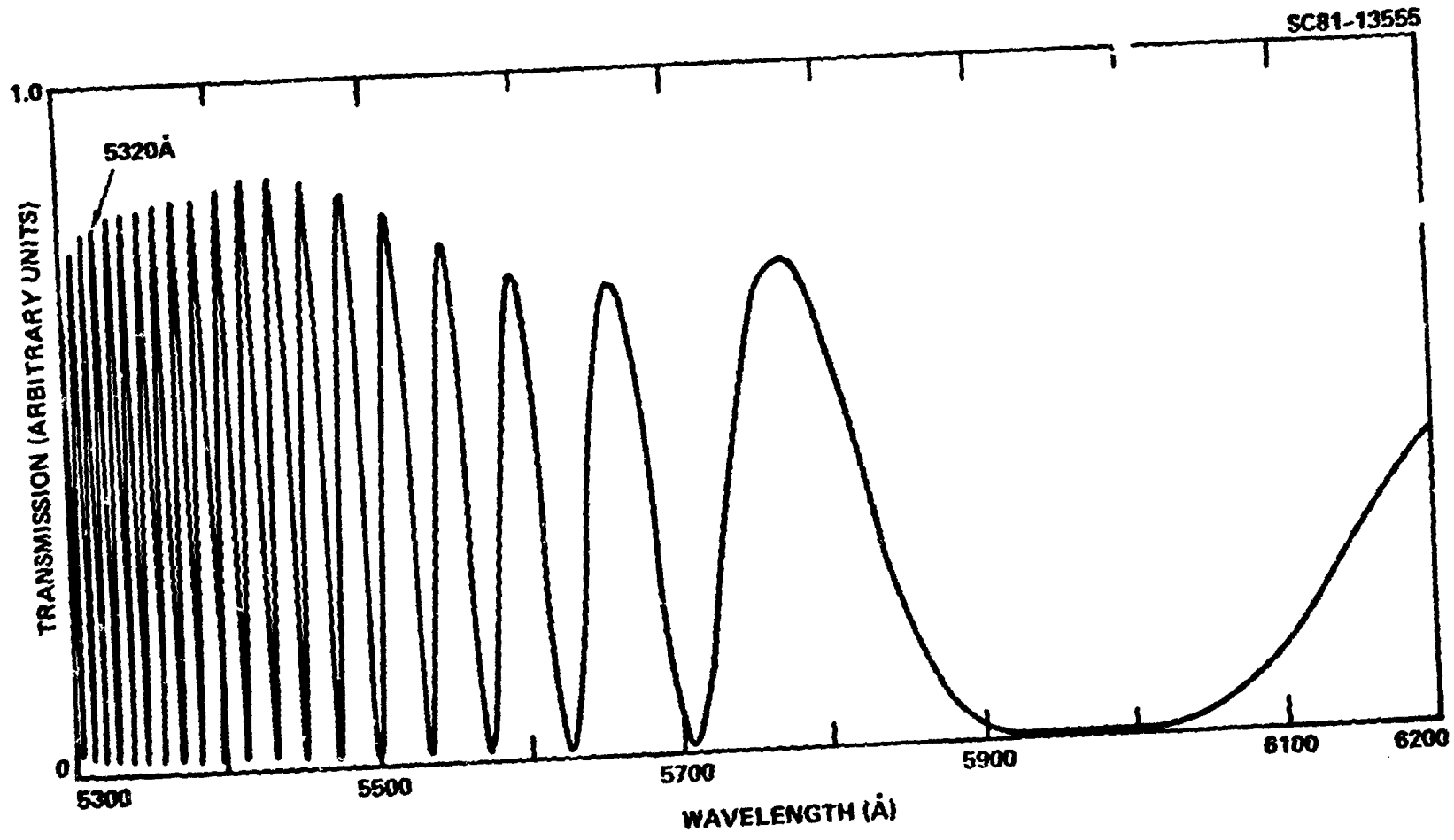


Fig. 12a Spectra of individual filter stages (a) 16th-order.

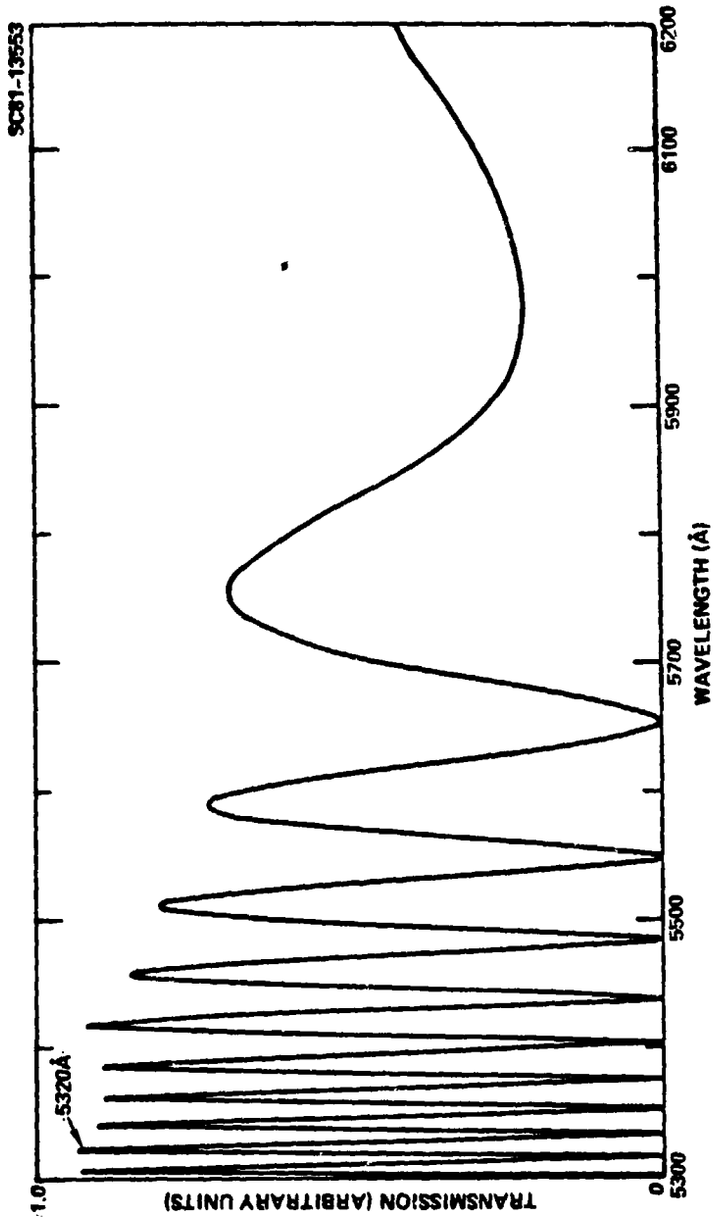


Fig. 12b Spectra of individual filter stages 8th-order.

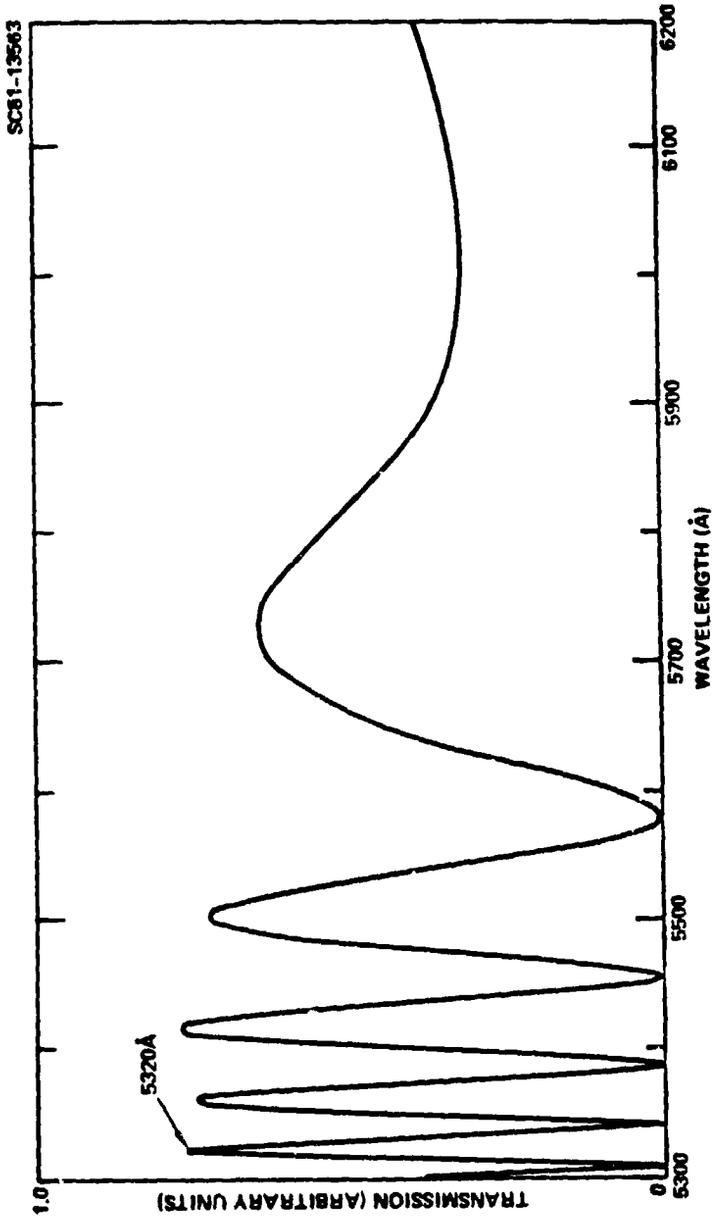


Fig. 12c Spectra of individual filter stages 4th-order.

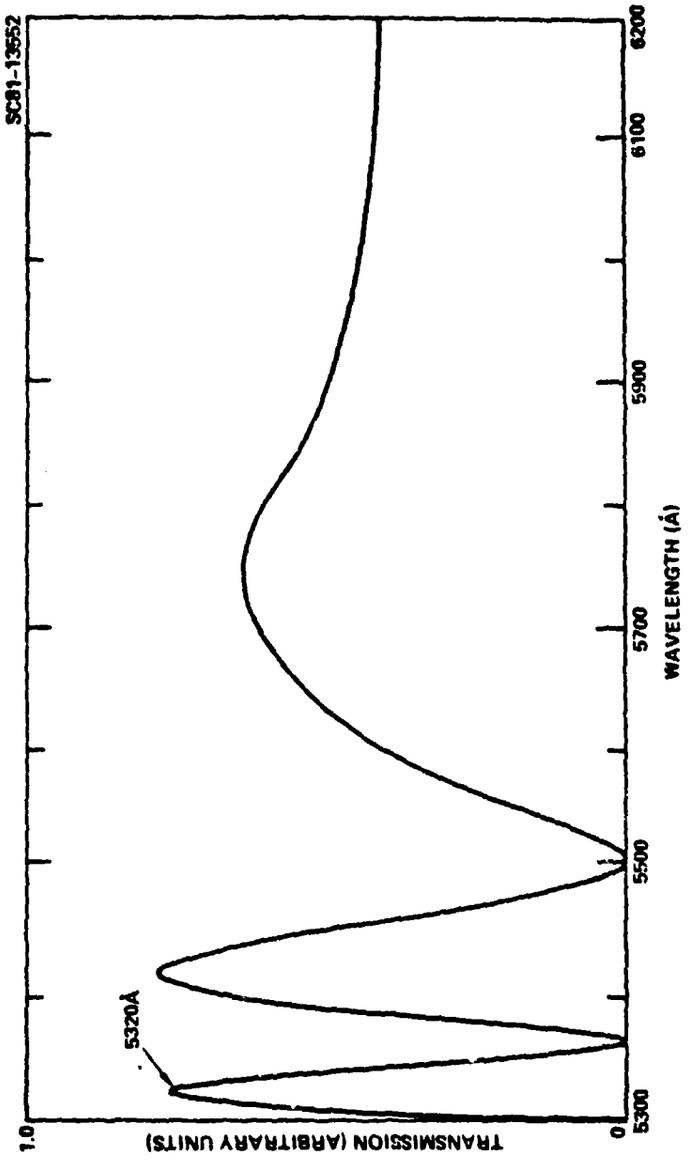


Fig. 12d Spectra of individual filter stages 2nd-order.

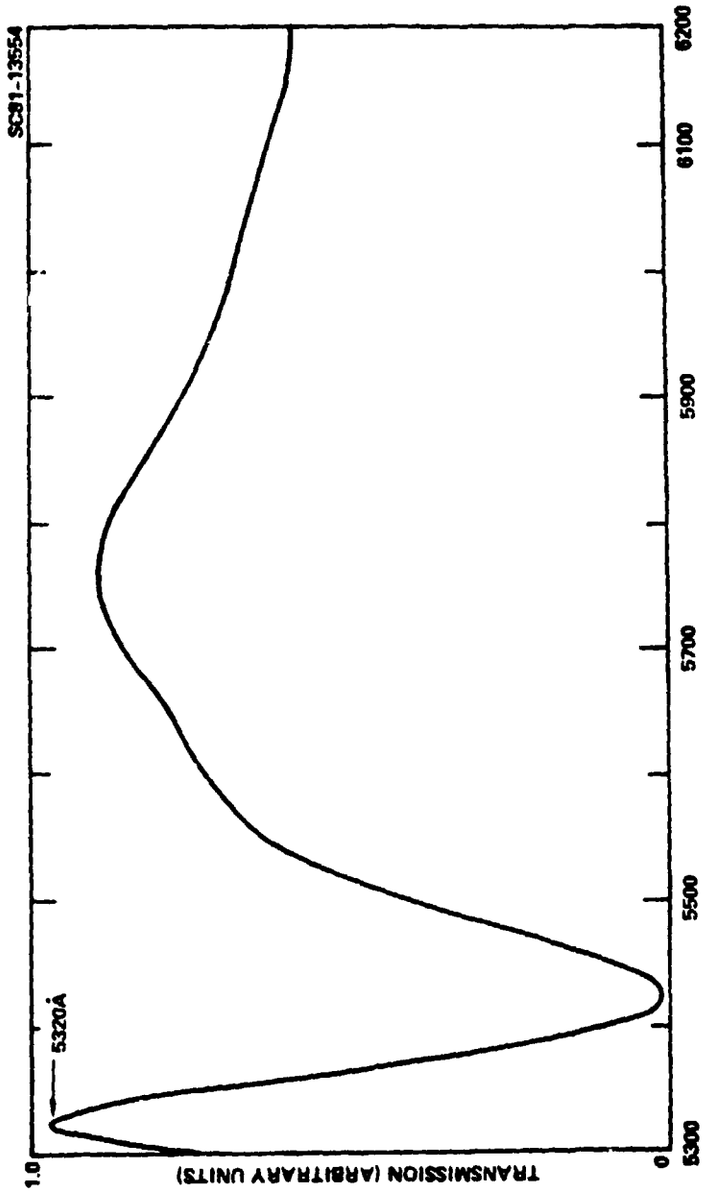


Fig. 12e Spectra of individual filter stages 1st-order.

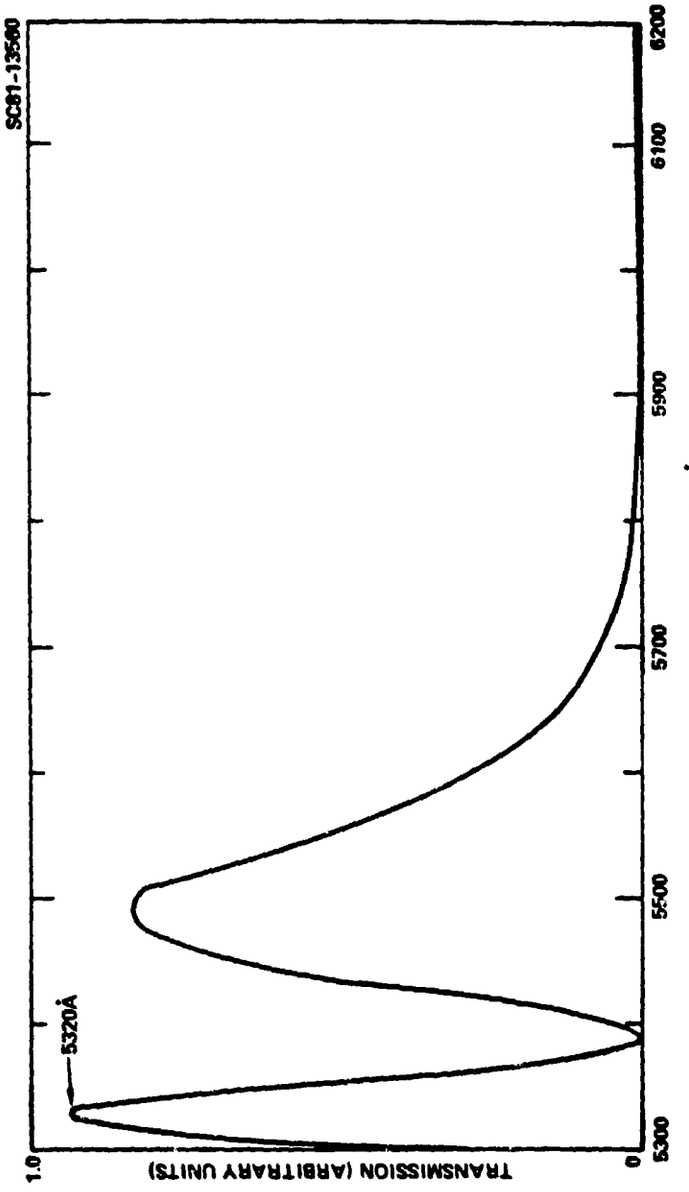


Fig. 12f Spectra of individual filter stages 1.5-order.

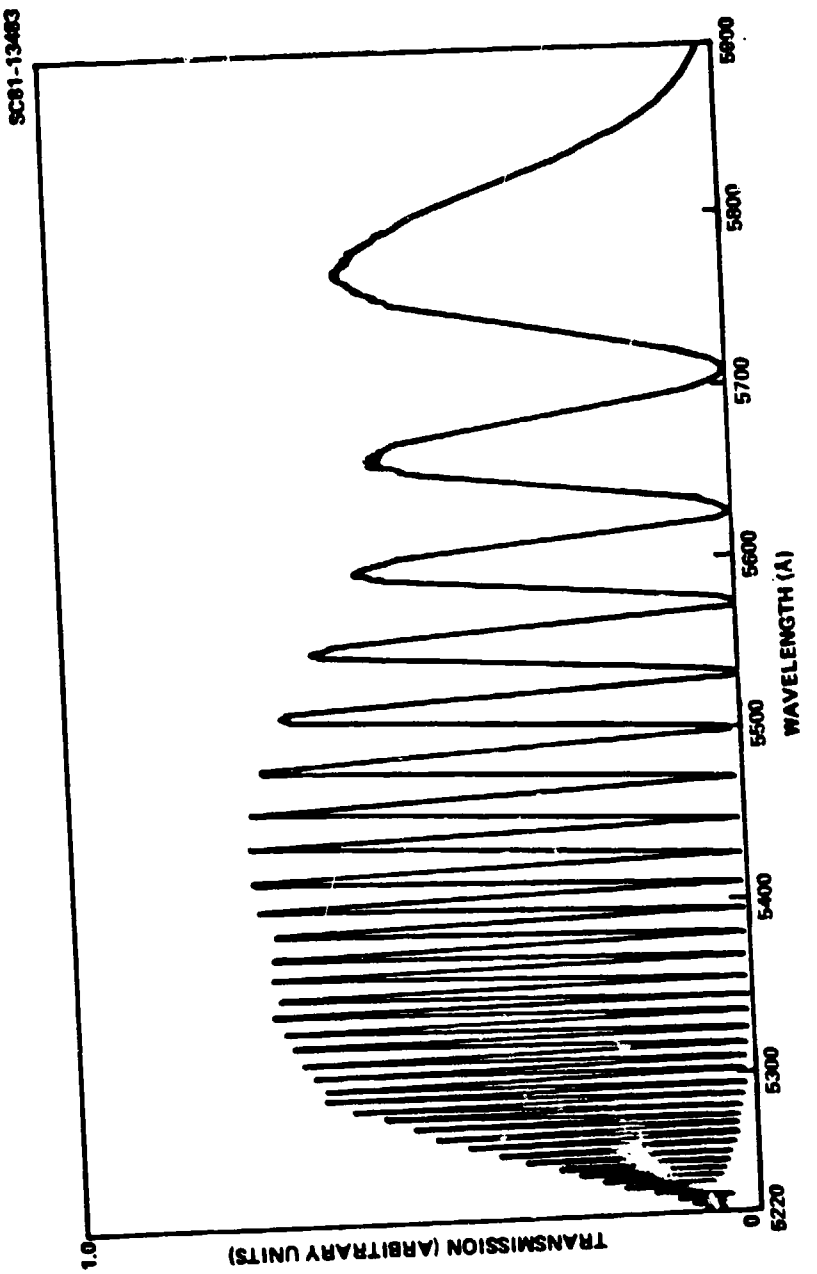


Fig. 13a Transmission of filter segments 16th-order.

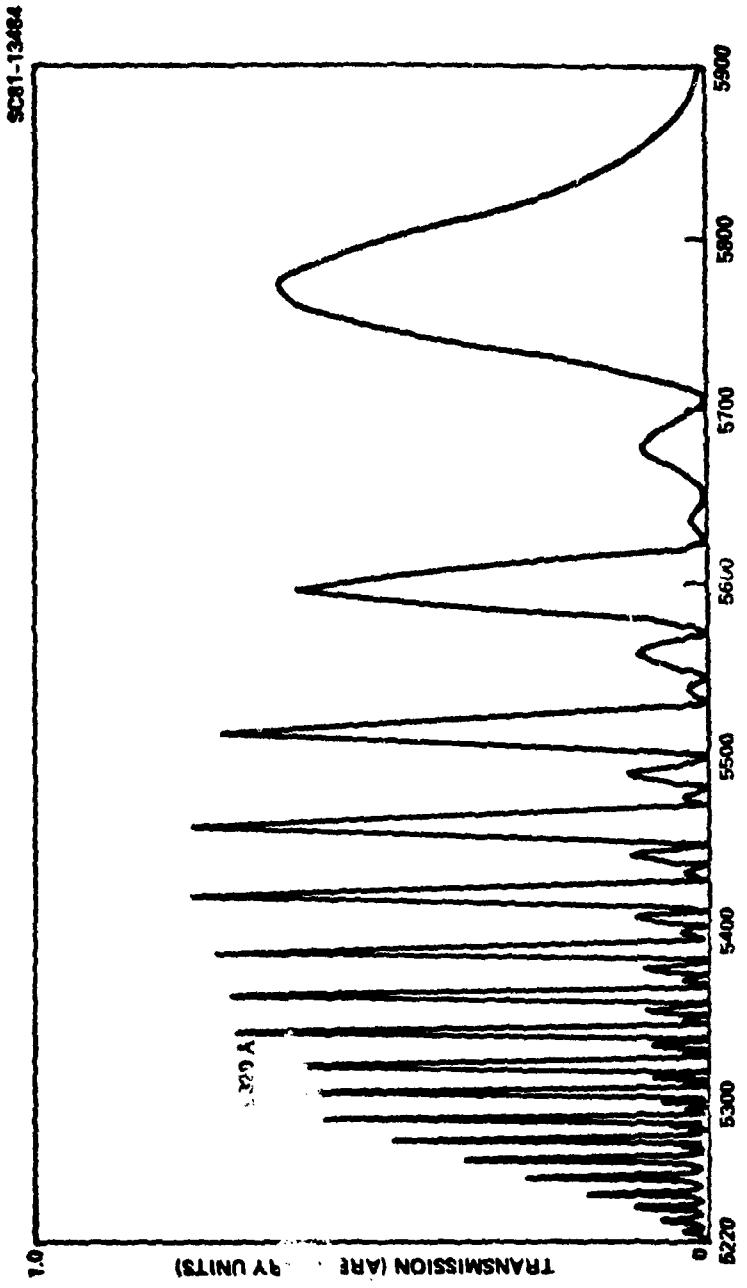


Fig. 13b Transmissio.. of filter segments 16:8-order.

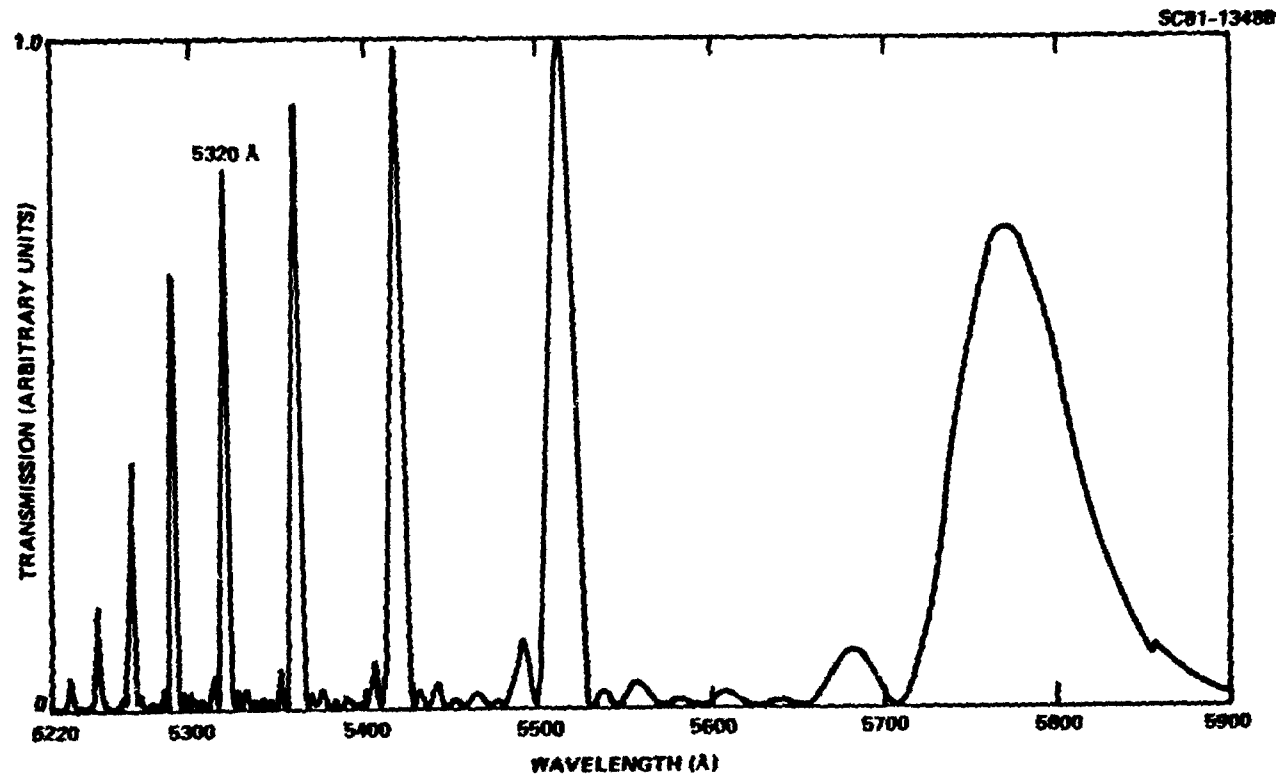


Fig. 13c Transmission of filter segments 16:8:4-order.

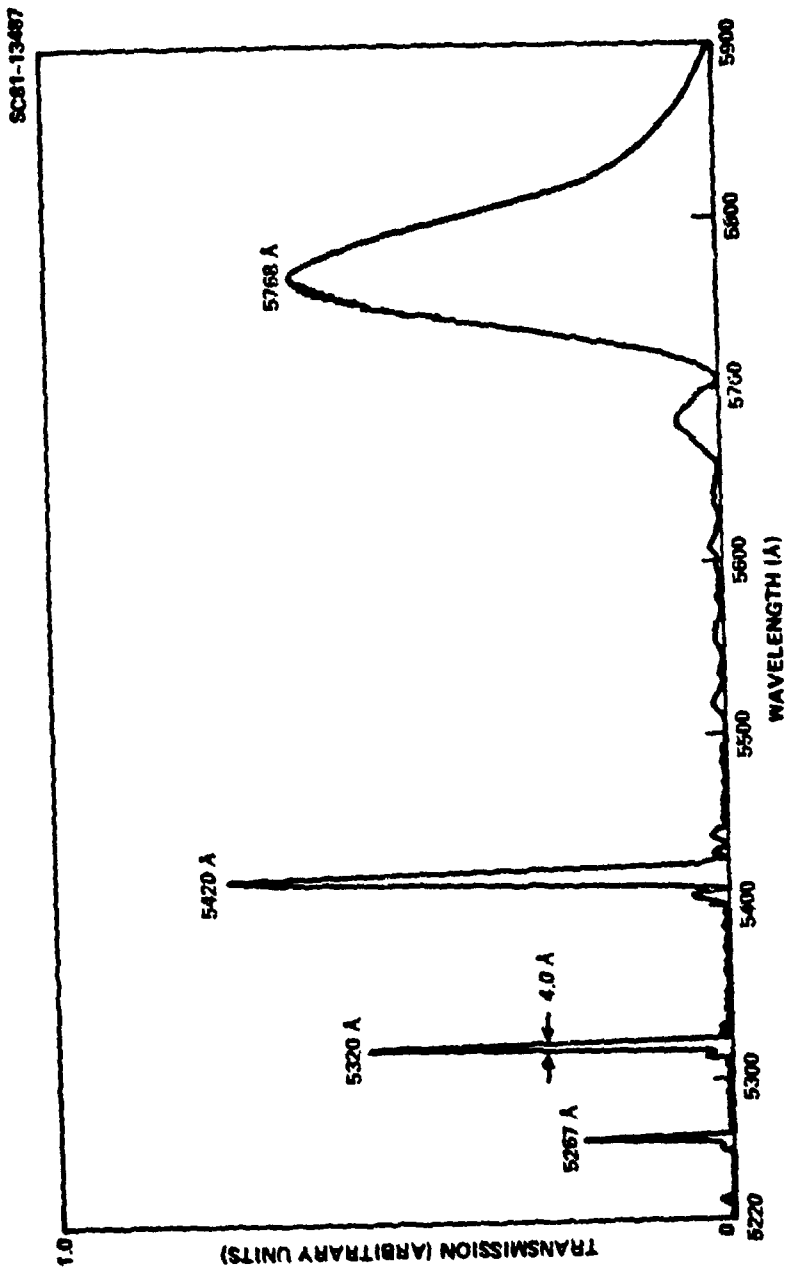


Fig. 13d Transmission of filter segments 16:8:4:2-order.

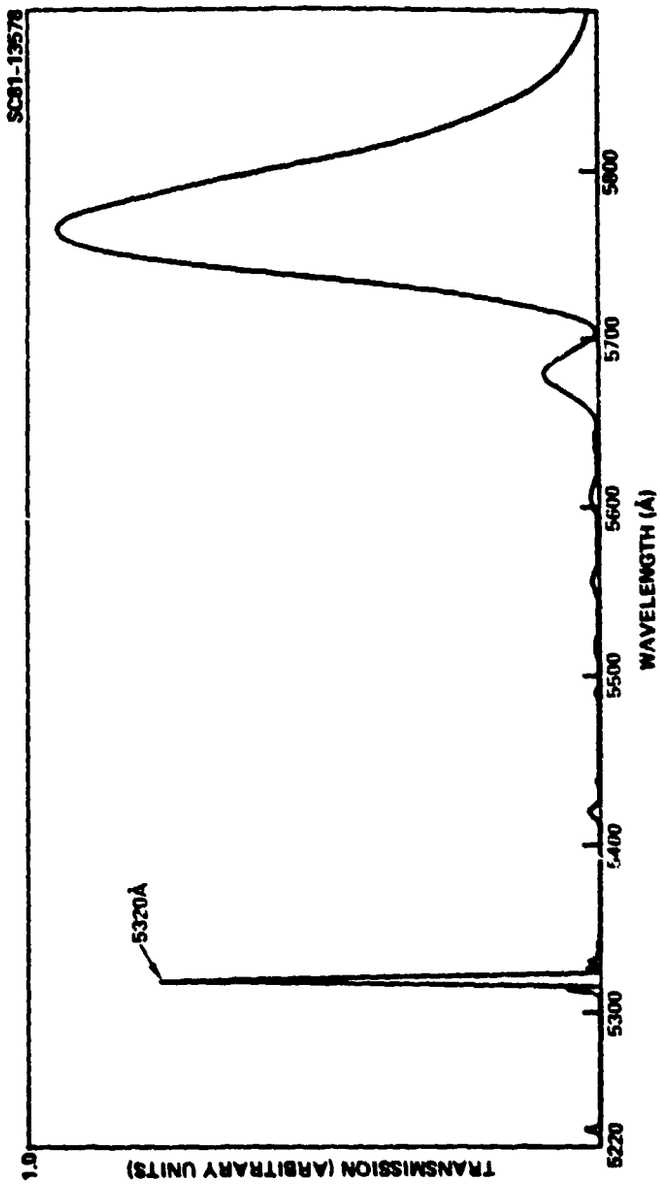


Fig. 13e Transmission of filter segments 16:8:4:2:1-order.

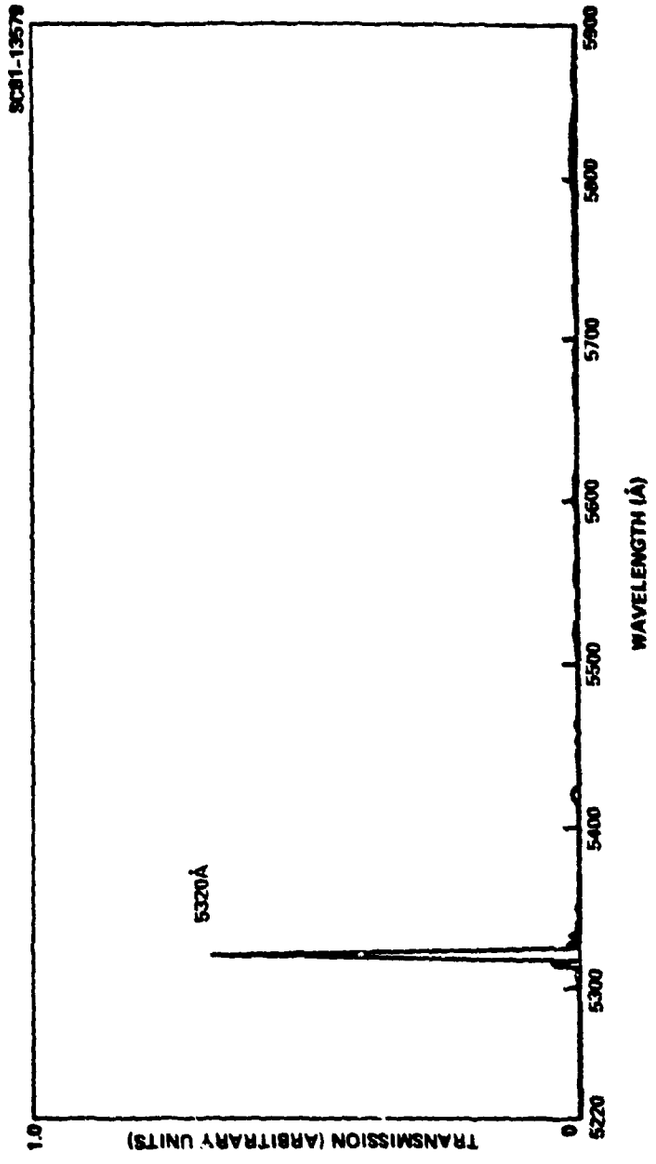


Fig. 13f Transmission of filter segments 16:8:4:2:1:1.5-order.

SC81-13920

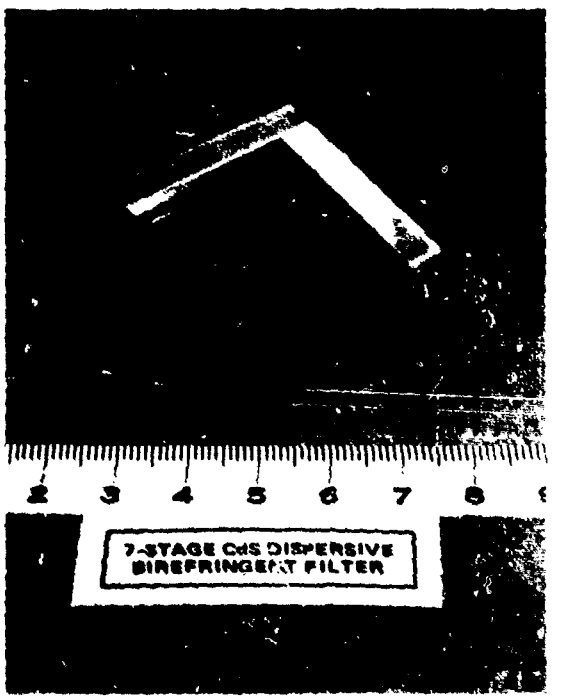


Fig. 14 Seven-stage CdS filter.

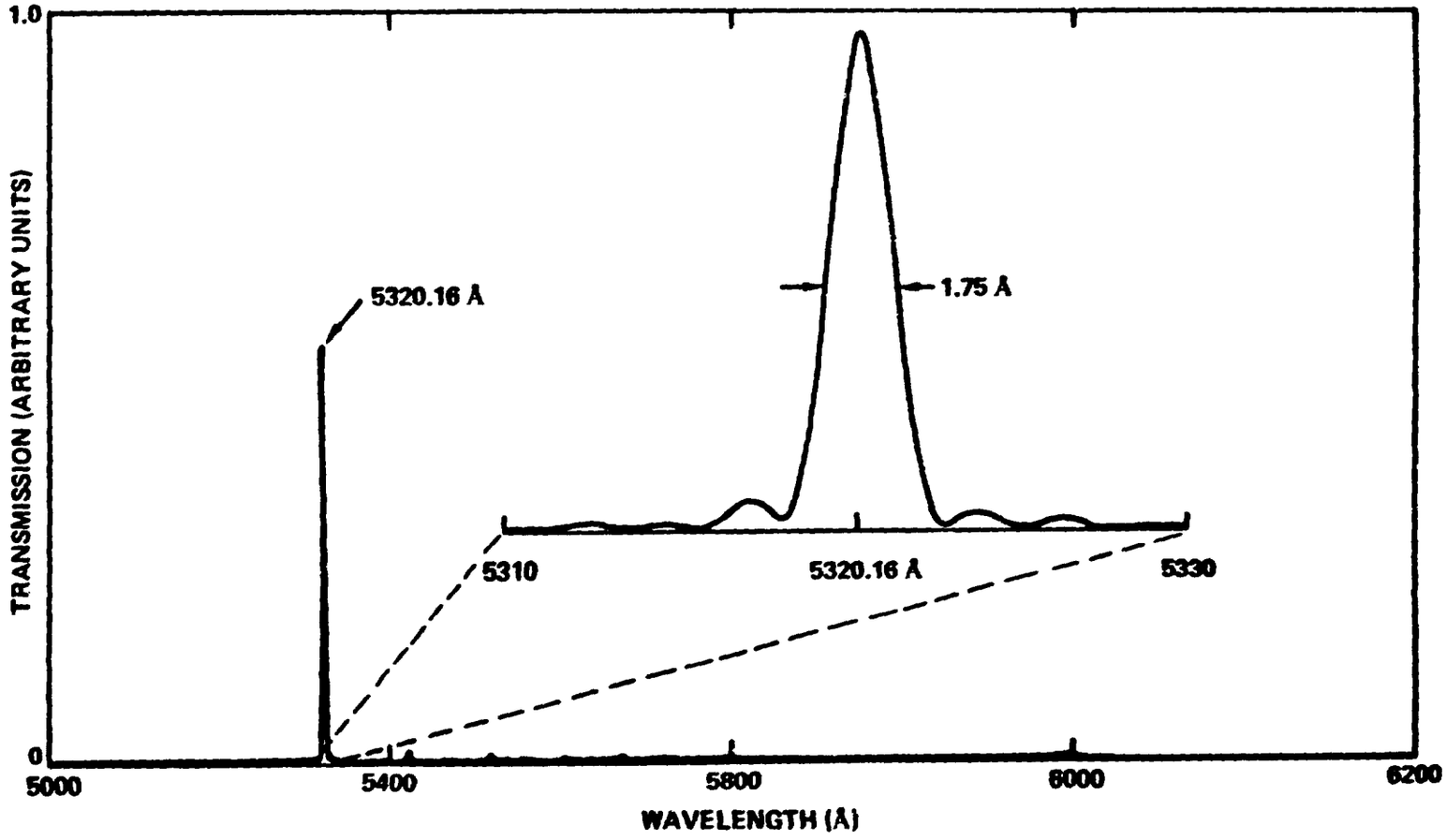


Fig. 15 Measured transmission of seven-stage CdS filter.

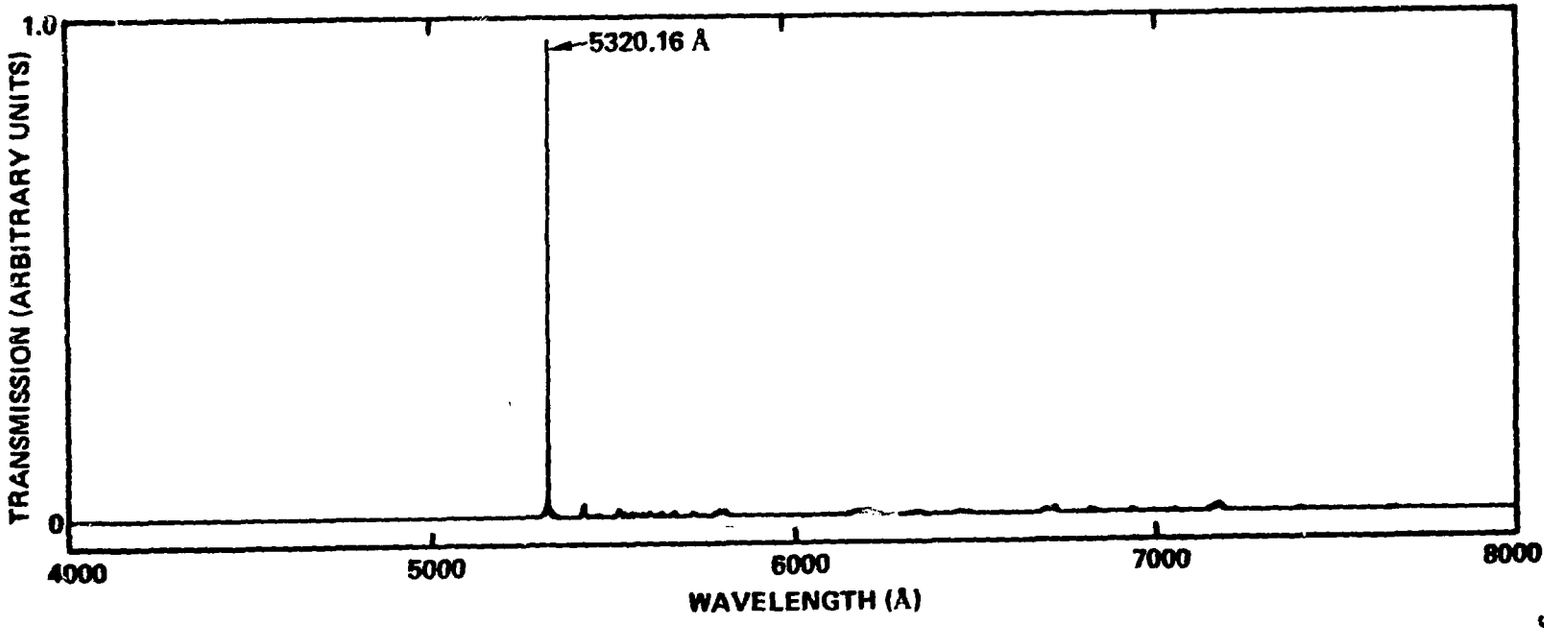


Fig. 16 Transmission of CdS filter over extended spectral range illustrating complete blocking in the visible.

peak position was 5320.2 A at ambient temperature with a FWHM of 1.75 A. Applying the temperature correction, mentioned above, results in a passband at 5320 A at 299K.

Peak transmission of the filter was quite low (on the order of a few percent). This was caused by the low transmission of the polarizers, lack of anti-reflection coatings, surface scattering, and possible increases in CdS bulk absorption over the published values used in the filter modeling. These issues will be discussed in more detail later in this report.

Since the baseline filter design was structured to achieve a FOV of ±60° in air, only the 32nd, 16th and 8th-order stages were to be constructed in the wide-field geometry. Therefore the 4th-order stage would determine the FOV. Figure 17 shows a series of measured transmission curves for a single interference peak of a fourth-order stage at several zenith angles. Using the earlier definition, we find a FOV of ±59°. This agrees quite well with our prediction of ±54° based on Eq. (14).

Field-of-view measurements were also made on various combinations of nonfield-widened filter stages. As expected, the measured spectral shift is in excellent agreement with predictions. The non-wide field filter has a measured FOV of ± 22°, in agreement with the predicted value. Therefore, even in its simple Lyot-Öhman configuration, the DBF has a greater FOV, and consequently potentially higher throughput than traditional filters of comparable bandwidth. It is important to recall the two-fold symmetry of the wide-field monochromatic fringes. This requires that the optic-axes of all of the CdS plates be parallel throughout the filter. Otherwise, at a given incidence angle, some stages would shift to longer, and others to shorter wavelengths, thus destroying the required interference between stages.

Other properties of these stages at large angles of incidence are discussed later, when the properties of polarizers at these angles are described.

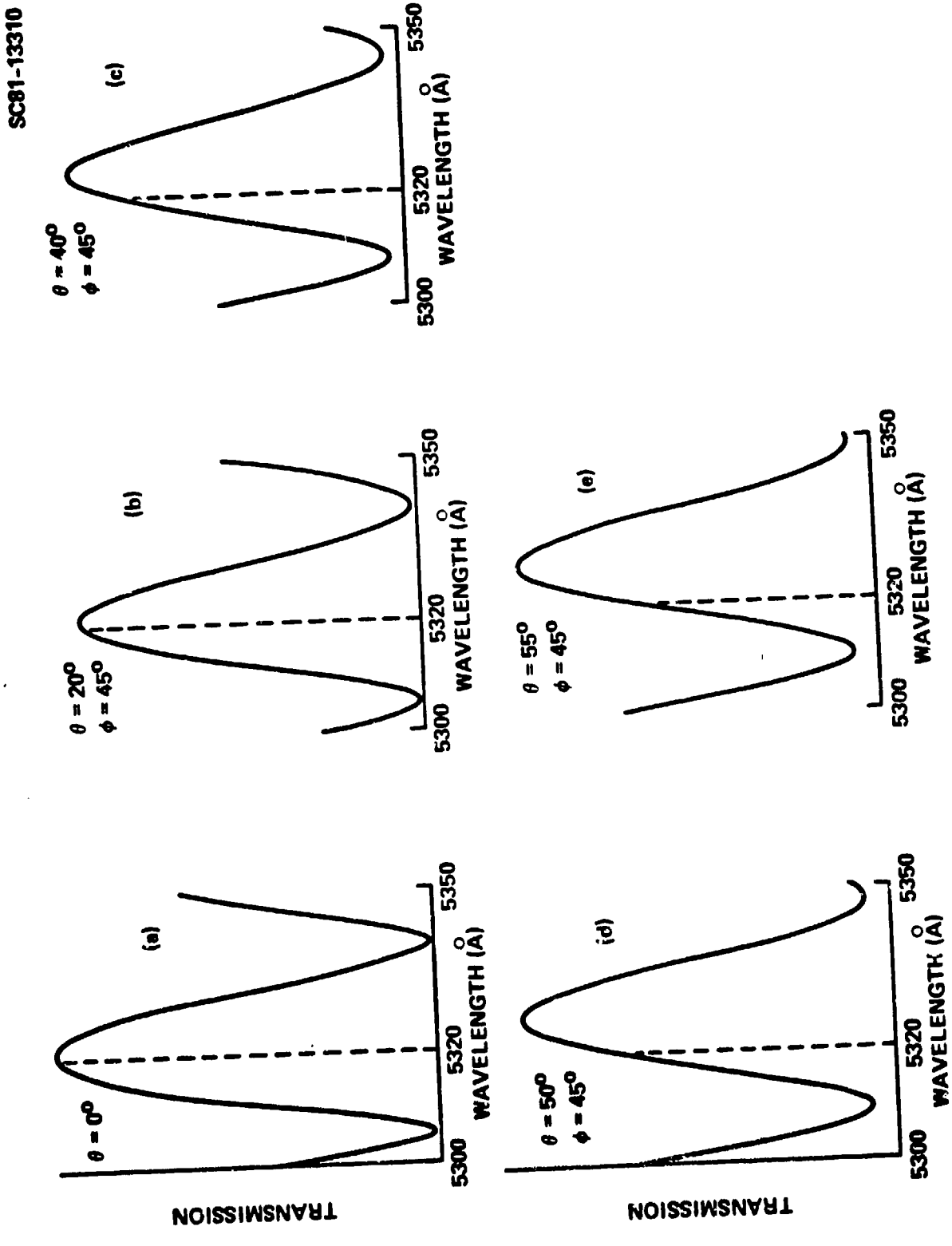


Fig. 17 Interference spectrum of 4th-order stage at various angles of incidence.

## 3.4 Lyot-1 Wide-Field Properties

Initial measurements have been performed on a field-widened stage. This configuration is of the Lyot-1[19] type illustrated in Fig. 3. In this geometry, rays which acquire an increased phase retardation in one plate experience a compensating decrease in the second plate. As a result, in addition to greatly increasing the FOV, the azimuthal dependence is removed. For this measurement, a piece of half-wave Polaroid waveplate material was stripped and laminated between two thin pieces of glass. Two equal thickness CdS crystals were positioned on either side of the waveplate and the assembly was rotated between a pair of fixed linear polarizers. Representative results are shown in Fig. 18 in which the birefringence interference spectrum of a single stage is plotted for several angles of incidence. These measurements were made at an azimuth which would have corresponded to the worst case angle for a nonfield-widened plate. In the nonfield-widened version, the FOV of the stage tested would have been ±28°. As expected no measurable spectral shift was observed out to the extreme angle of 60°. The overall decrease in transmission with incidence angle was caused by vignetting, since a small aperture was used in this measurement.

Some of the peculiar features which were observed in the course of these measurements have served to further illustrate some of the features of these birefringence element configurations. As a result of the modeling, discussed below, each of these effects has been attributed to misalignment of various elements in the structure. For example, the modulation of peak-to-peak intensity observed in Fig. 18 has been determined to be caused by misorientation of the CdS elements.

Earlier workers have done extensive studies of the effects of errors in wide-field stages.[4] In filters fabricated using traditional materials, such as quartz and calcite, the errors readily become apparent as distortions of the wide-field monochromatic fringe patterns. Therefore, visual inspection of these stages is adequate for determining the source of the error and for guiding corrective measures.

SC81-12520

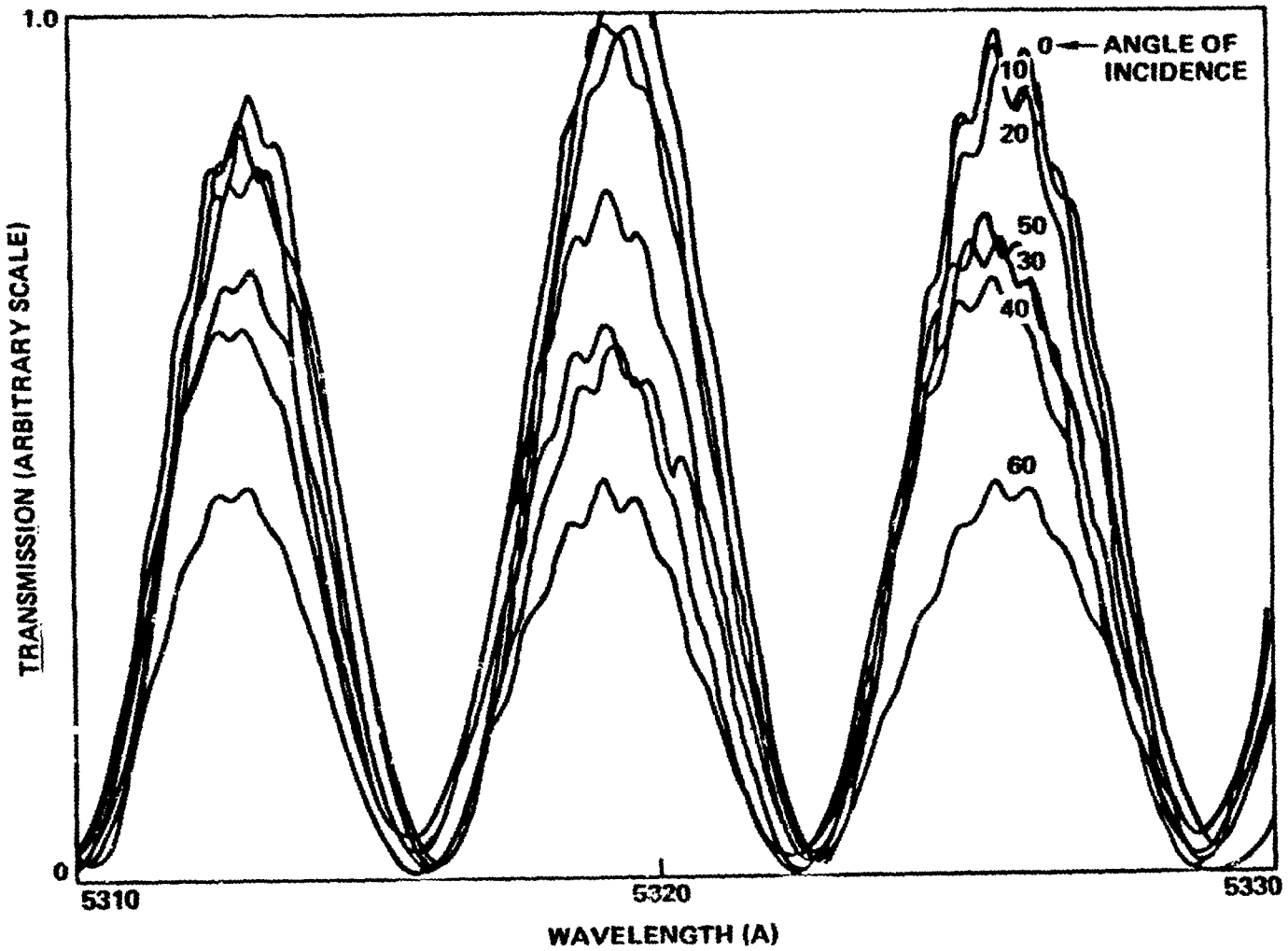


Fig. 18 Interference spectrum of CdS Lyot-1 filter stage at various angles of incidence.

The situation for DBF wide-field stages is not so easily analyzed. Because of the large fields-of-view encountered, wide-field fringe patterns cannot be easily observed. Careful modeling of the effects of errors on the spectral properties at normal incidence does lead to an approach for determining errors in alignment in Lyot-1 stages. A computer program was generated for calculating the spectral properties of arbitrary combinations of waveplates and polarizers using the traditional Jones calculus formalism. Spectral scans for a 32nd-order Lyot-1 stage were calculated for various combinations of alignment errors. A tabulation of various errors, and their qualitative effects on the normal incidence spectrum, is presented in Table 2 below. To verify these predictions, a 32nd-order Lyot-1 stage was assembled and deliberate alignment errors were introduced. In each case, as seen in Fig. 19, similar qualitative effects are observed in the calculated and measured spectra. The measured spectrum, in the absence of alignment errors, showed little peak-to-peak modulation, but the minima did not approach zero. A measurement of the half-waveplate used in this experiment indicated that the half-wave wavelength was located at 5950 Å, far removed from 5320 Å, which accounts for the lack of complete extinction in the assembled stage.

Table 2

Effects of Alignment Errors on the Normal Incidence Spectrum of Lyot-1 Filter Stages

| Error | Effect |
|---|---|
| 1. $\lambda/2$ plate misaligned | - Decrease in transmission |
| 2. One crystal plate misaligned | - Modulation of both maxima and minima |
| 3. Both crystal platesmisaligned in same direction | - Modulation of maxima only |
| 4. Both crystal plates misaligned in opposite sense | - Modulation of minima only |

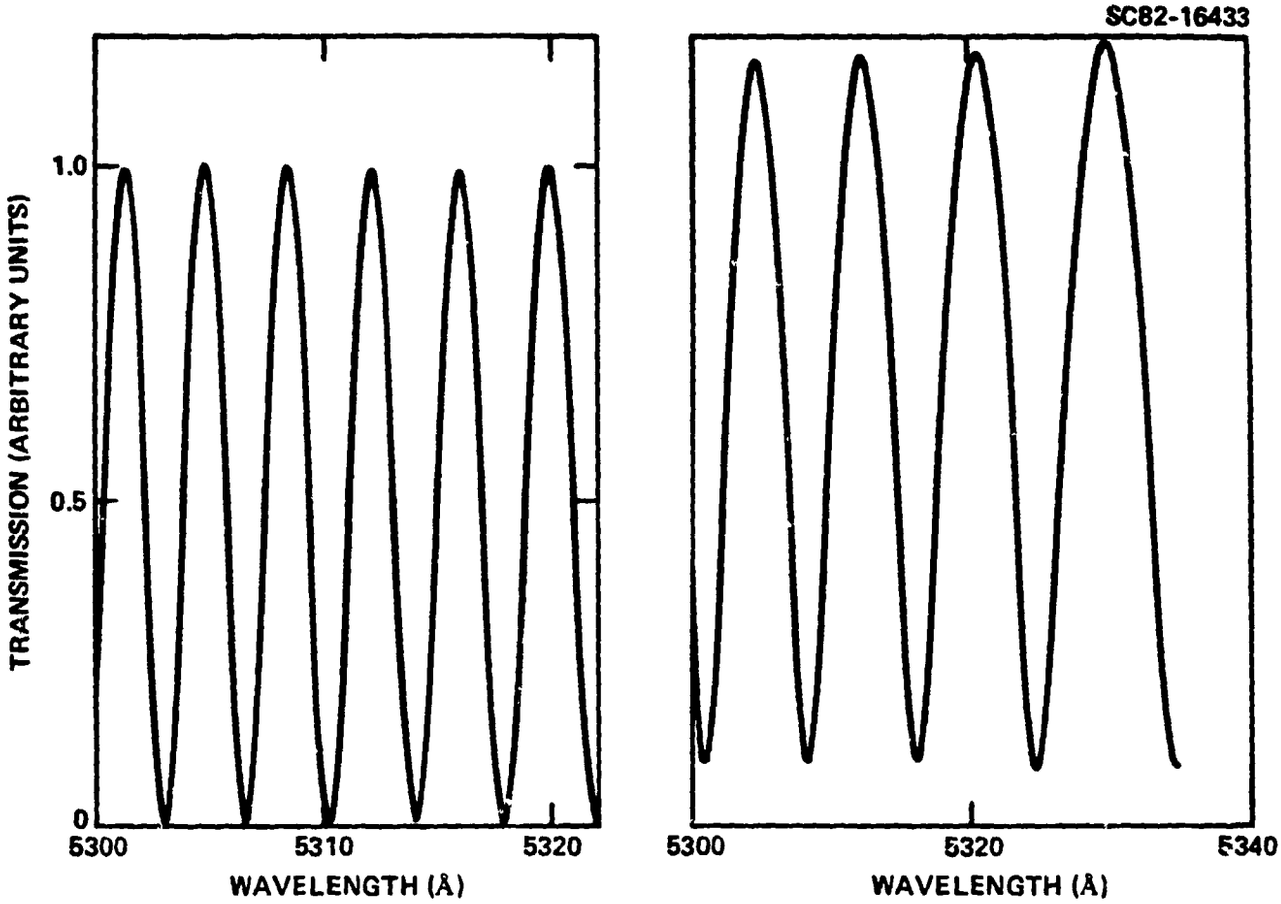


Fig. 19a Effects of plate misalignment errors on the normal incidence spectrum of Lyot-1 filter stages, calculated and measured. All plates in proper alignment. Measured data show poor extinction since λ/2-plate was not half-wave at 5320 Å.

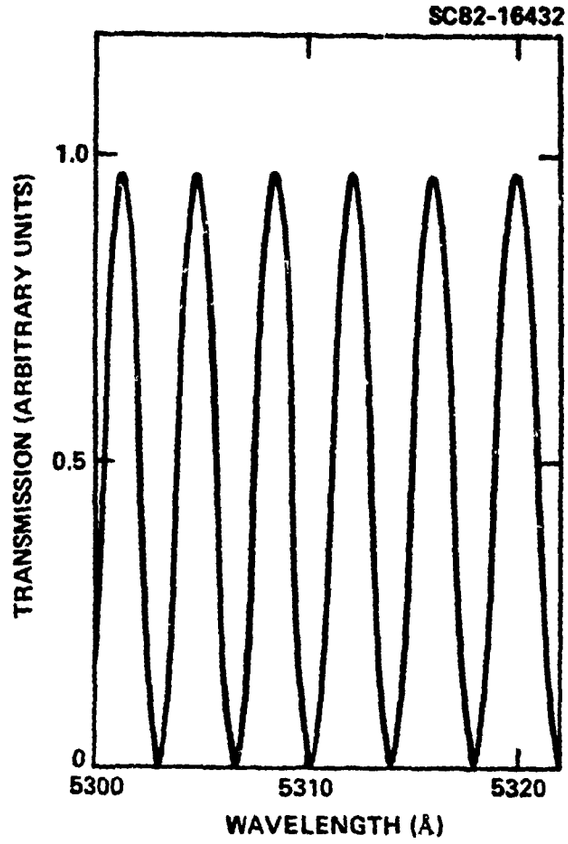


Fig. 19b Effects of plate misalignment errors on the normal incidence spectrum of Lyot-1 filter stages, calculated and measured. λ/2-plate misaligned. Measured results not shown since the uniform drop in transmission is difficult to discern when presenting relative measurements.

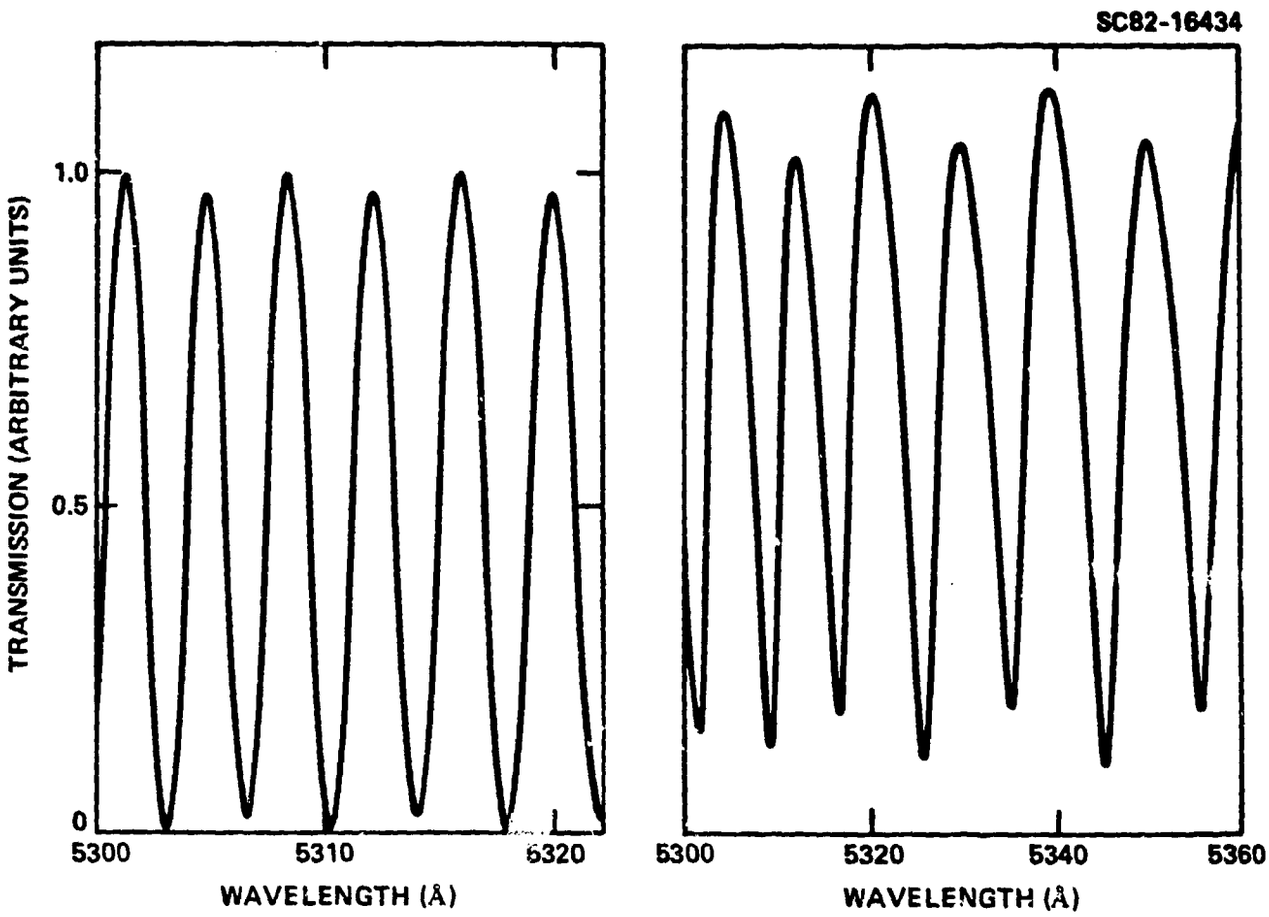


Fig. 19c Effects of plate misalignment errors on the normal incidence spectrum of Lyot-1 filter stages, calculated and measured. One crystal plate is misaligned.

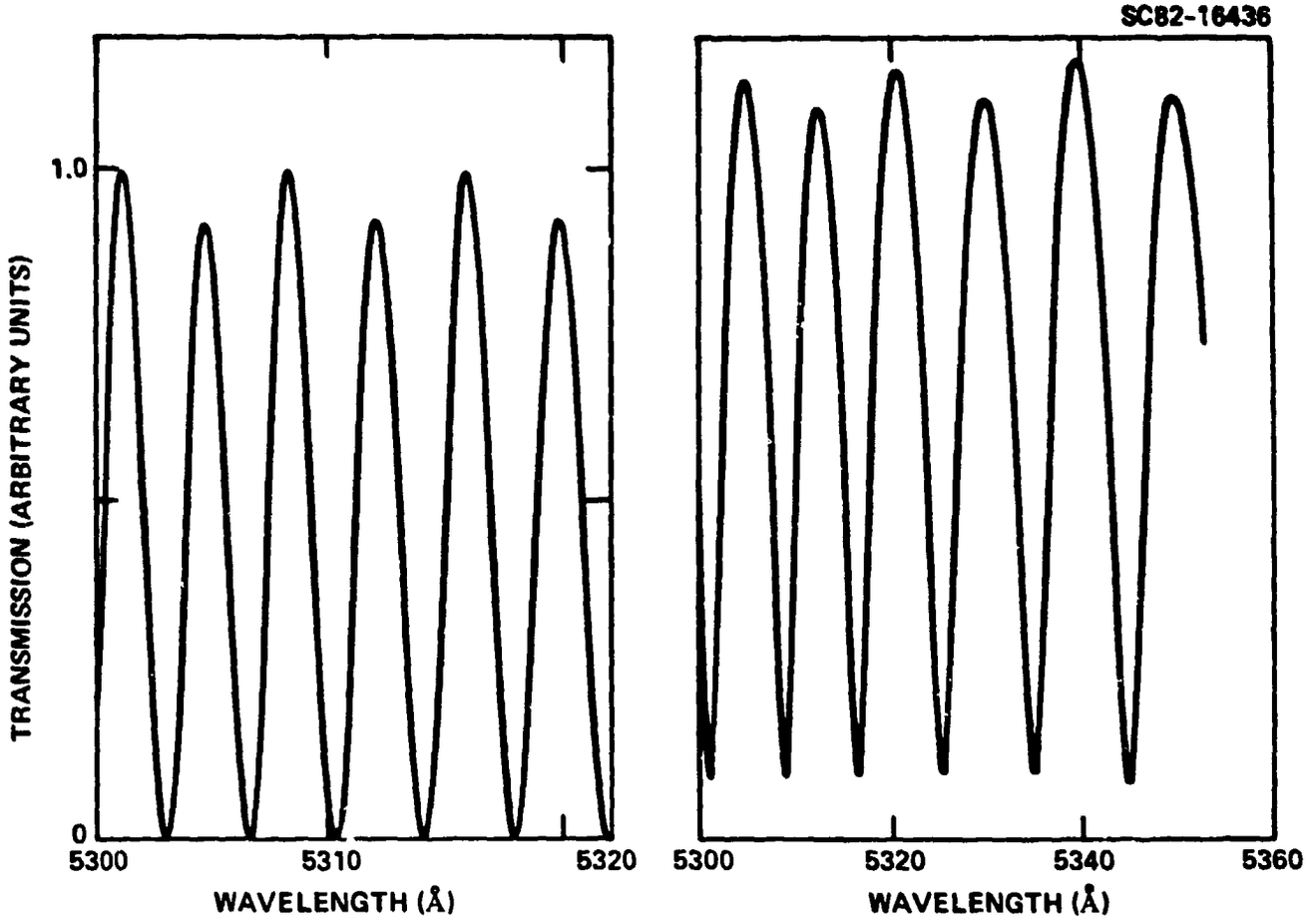


Fig. 19d Effects of plate misalignment errors on the normal incidence spectrum of Lyot-1 filter stages, calculated and measured. Both crystal plates misaligned in same direction.

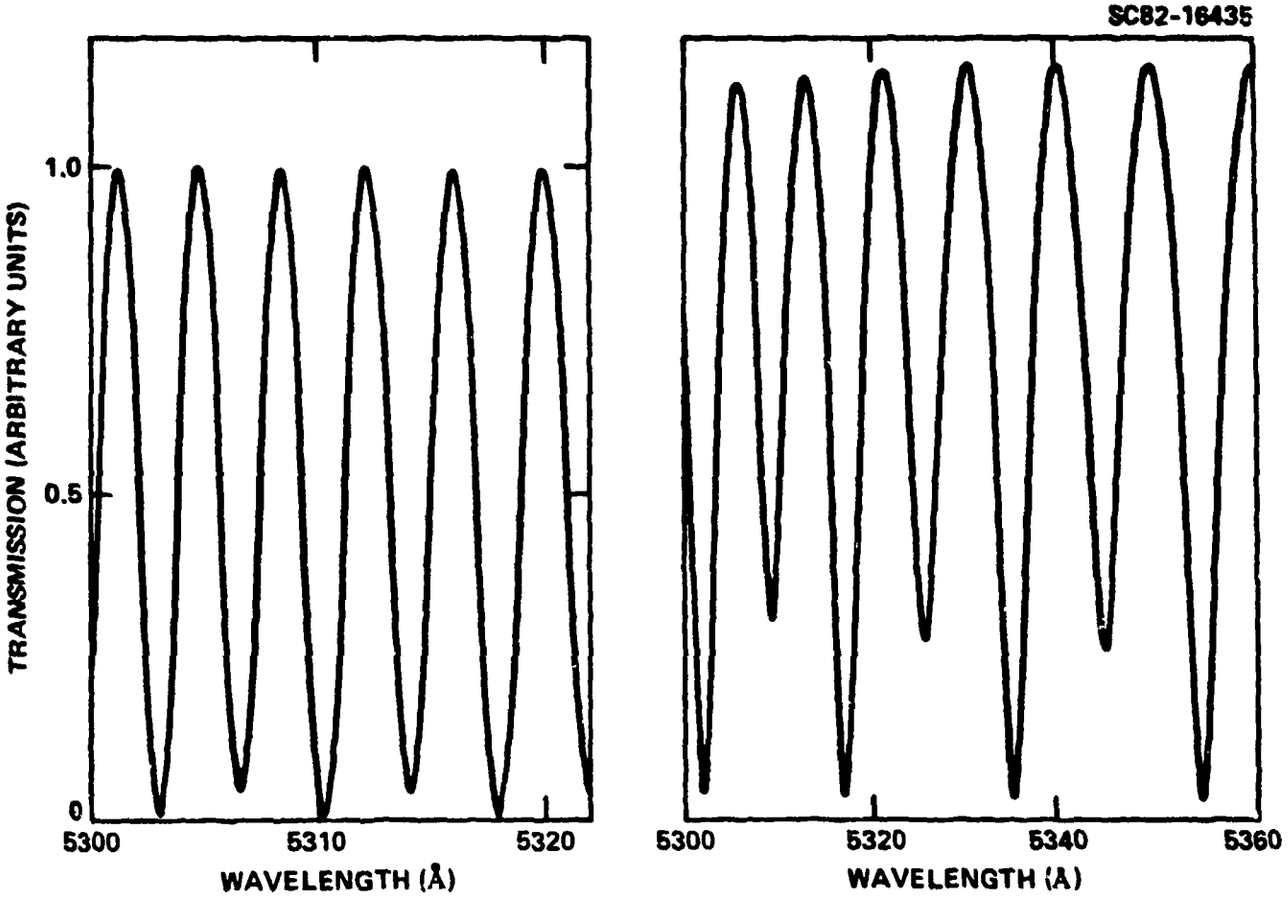


Fig. 19e Effects of plate misalignment errors on the normal incidence spectrum of Lyot-1 filter stages, calculated and measured. Both crystal plates misaligned in opposite directions.

Therefore, we have found that it is possible to analyze, and therefore correct for alignment errors in wide-field stages by studying the structure of the normal incidence transmission spectrum.

## 3.5 Effects of Polarizers at Large Incidence Angles

Most optical devices which employ polarizers are designed to operate with rather restricted fields-of-view (f/3 or less). Over such a range of incident angles, the polarization properties of sheet polarizers do not vary significantly from their normal incidence values. However, at the large angles for which a DBF is designed, polarizers are required to operate in a regime where their extinction efficiency is degraded.[37] This degradation is dependent on azimuth angle. If the polarizers are rotated about an axis parallel, or perpendicular, to the polarization axes, no degradation is observed. The decrease of extinction becomes a maximum for planes of incidence at 45° to the polarization axis. This effect appears to have been overlooked by other workers in their development of wide field-of-view filters.

The origin of the polarizer degradation is two-fold. First, the Fresnel reflection at an interface causes a small rotation of the plane of polarization of the transmitted wave at large angles of incidence. This effect can easily be demonstrated by rotating a pair of crossed polarizers in a collimated beam. At large angles of incidence where extinction is degraded, the transmission can be slightly reduced by rotating the polarizers away from their crossed orientation. Yeh[37] has argued that this rotation can be minimized by index matching of each surface to eliminate the index discontinuity.

The second cause of polarizer degradation can be understood if the polarizer material is thought of as a dichroic uniaxial crystal. To model this situation, the ordinary index is assumed to be real, while the extraordinary index is complex, and hence lossy. As light enters at large angles of incidence, the value of the extraordinary index approaches the real lossless ordinary value.

Several measurements were performed to determine the effects of polarizer degradation on filter performance. The extinction of a pair of crossed polarizers was measured at an angle of incidence of 50°, at the worst case azimuth. The transmission was found to be 18%. In contrast, the intensity of interference minima of a single filter stage, in which the index discontinuity was reduced by anti-reflection coatings and an index matching fluid, was only 4%.

Contributions of the polarizers in additional filter stages should result in an extinction of out-of-band light which is acceptable at the largest angles. This was studied by measuring several multiple stage combinations at large angles of incidence. Representative spectral scans of the sideband structure a three-stage filter, at normal incidence and at $\theta = 40°$, are shown in Fig. 20. As expected, no real change appears in the sideband structure for rotations in the plane containing the polarization axis ($\phi = 0°$ and 90°). However, at an azimuth of $\phi = 45°$ additional intensity appears and the central minimum disappears. This is expected, as the central minimum is the result of extinction produced by a single filter stage while the other minima are the result of multiple extinctions. The overall increase of sideband intensity appears to be quite small, and justifies our assumption that multiple polarizer structures will tend to be relatively immune from the effects of wide-field polarizer degradation. This is an important conclusion, since other wide-FOV filters[7] rely on the extinction produced by a small number of polarizers (2 or 3), and as such may have considerable out-of-band transmission at large fields-of-view. Our earlier comment, regarding the determination of optimum filter design, is related to this property of polarizers. Many birefringent filter configurations promise better sideband suppression or tailoring of bandpass characteristics. However, these structures make use of a small number of polarizers, and therefore, result in increased out-of-band intensity at large angles of incidence.

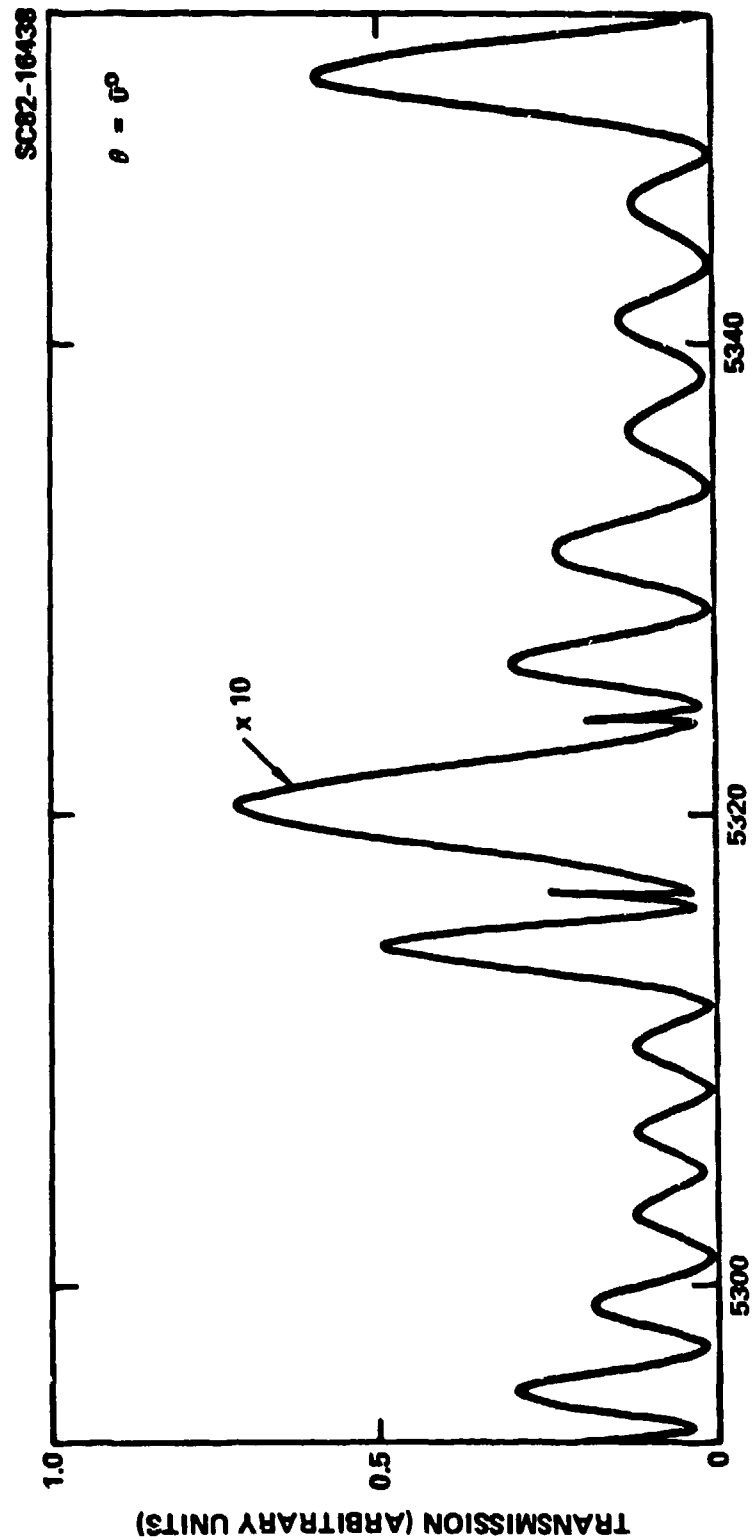


Fig. 20a Effect of incidence angle on the sideband structure of a 3-stage filter spectrum. Normal incidence.

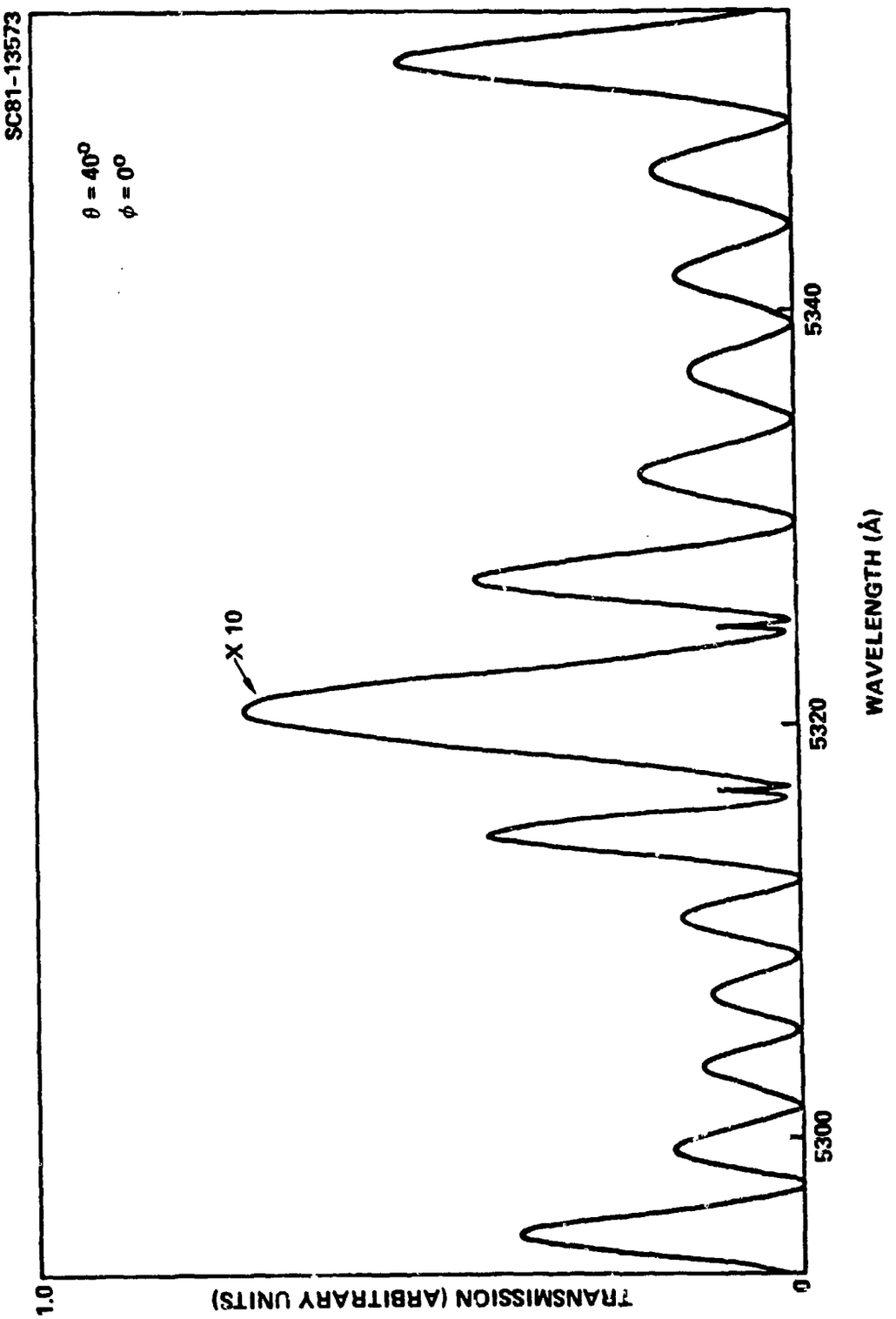


Fig. 20b Effect of incidence angle on the sideband structure of a 3-stage filter spectrum. 40° incidence angle at 0° azimuth.

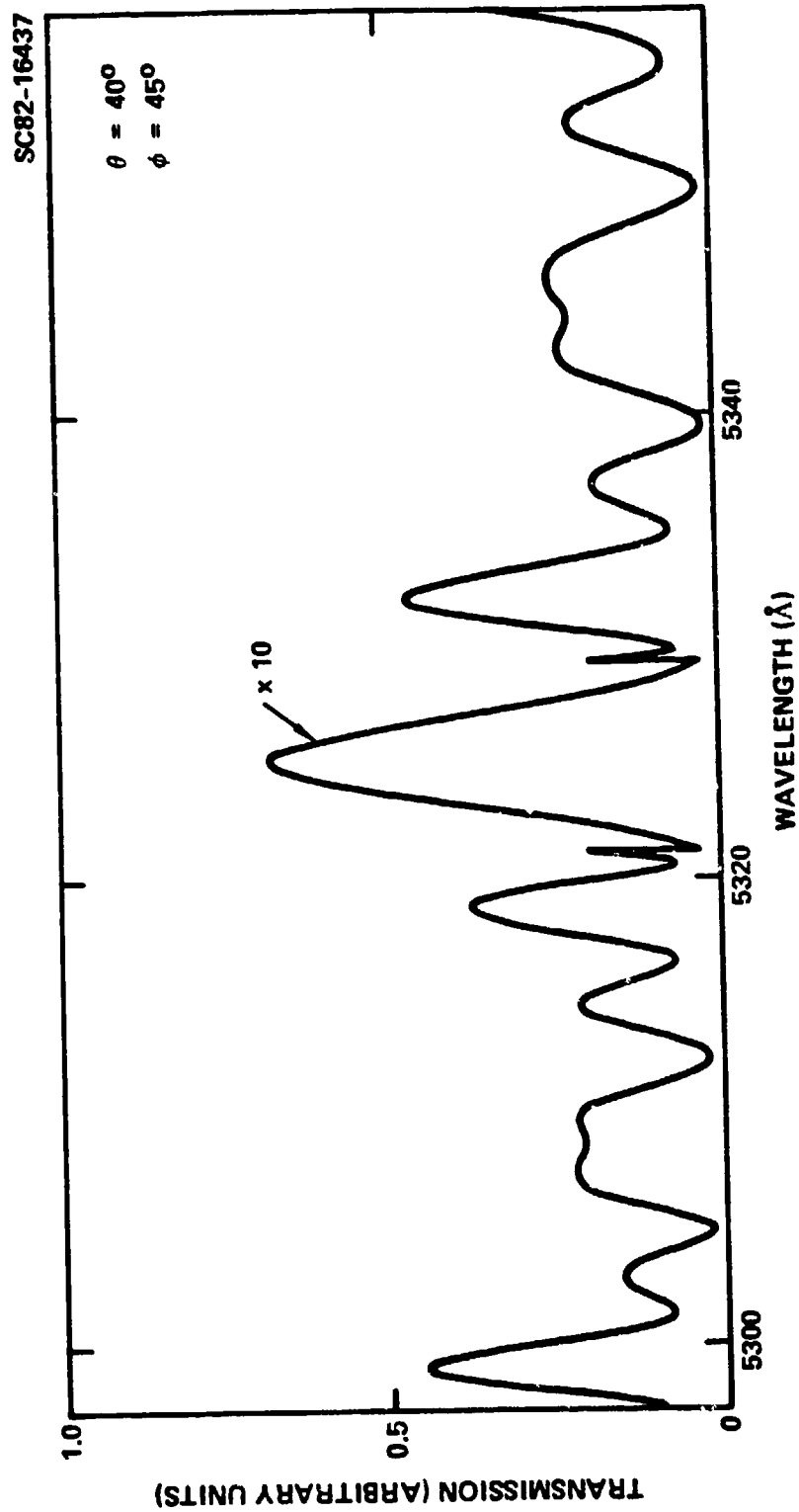


Fig. 20c Effect of incidence angle on the sideband structure of a 3-stage filter spectrum. 40° incidence angle at 45° azimuth. Azimuth angles are measured with respect to the polarizer axis orientation.

## 3.6 Wide-Field Half-Waveplates

In our discussion of wide-field filter stages, the half-wave element was a simple sheet of Polaroid half-wave polyvinylalcohol (PVA). While the field-of-view of this element is large, departures from half-wave retardation at large angles causes an increase in transmission at the minima of the interference spectrum. To extend the FOV of this element, a compound half-wave plate has been designed. It is fabricated using two birefringent plates, having opposite signs of birefringence.[17] Oriented with their optic-axes parallel, the angular dependence of their combined retardation is very nearly cancelled. The retardation is equal to the difference of the retardations of the individual plates, and is designed by choosing appropriate plate thicknesses to be half-wave at the desired wavelength.

The optimum parameters for a wide-field half-wave plate are determined by the following procedure. Equation (23) gives the approximate angular dependence of the phase retardation of a birefringent plate, where $\theta$ is the angle of incidence and $\phi$ is the azimuth angle.

$$\Gamma = \frac{2\pi\Delta nd}{\lambda}\left[1 - \frac{\sin^2\theta}{2n_o n_e}\left(1 - \frac{n_e + n_o}{n_e}\sin^2\phi\right)\right] \tag{23}$$

For the combination to be half-wave, we require $\Gamma_1 + \Gamma_2 = \pi$. To minimize the angular dependence, the following condition must be satisfied.

$$\frac{\Delta n_1 d_2}{n_1^2} = -\frac{\Delta n_2 d_2}{n_2^2} \tag{24}$$

This leads to the condition for a wide-field half-wave plate

$$d_1 = \frac{\lambda}{2\Delta n_1} \frac{n_1^2}{n_1^2 - n_2^2}$$

$$d_2 = \frac{\lambda}{2\Delta n_2} \frac{n_2^2}{n_2^2 - n_1^2} \quad . \tag{25}$$

If we choose sapphire and Polaroid PVA as the negative and positive materials respectively, we obtain

$$d_1(\text{sapphire}) = 97\ \mu m \text{ and } d_2(\text{PVA}) = 100\ \mu m \quad . \tag{26}$$

Since Polaroid full-wave PVA is roughly 82 μm in thickness, the sapphire thickness must be modified to produce half-wave retardation at 5320 Å. This small shift from optimum conditions is predicted to produce acceptable increases in the angular sensitivity.

The angular dependence of the phase retardation of these elements has been modeled using the exact expression for $\Gamma(\theta,\phi)$, Eq. (11). The calculated value of the phase retardation was transformed into its order of interference so that a perfect half-wave plate has a value of 0.50. Figure 21 shows the phase shift of a simple half-wave PVA plate plotted vs azimuth angle in one quadrant, for values of incidence angle ranging from 0° to 50°. In contrast Fig. 22 shows the results of a similar calculation for a compound PVA-sapphire waveplate, which assumes the use of the available Polaroid full-wave sheet. The maximum shift in phase retardation is reduced by a factor of seven. This should enhance the wide-field extinction of the Lyot-1 stages.

As of this writing, sapphire plates have been ordered for testing the large FOV wave-plate concept, but have not yet been received. This effort will continue under alternate support.

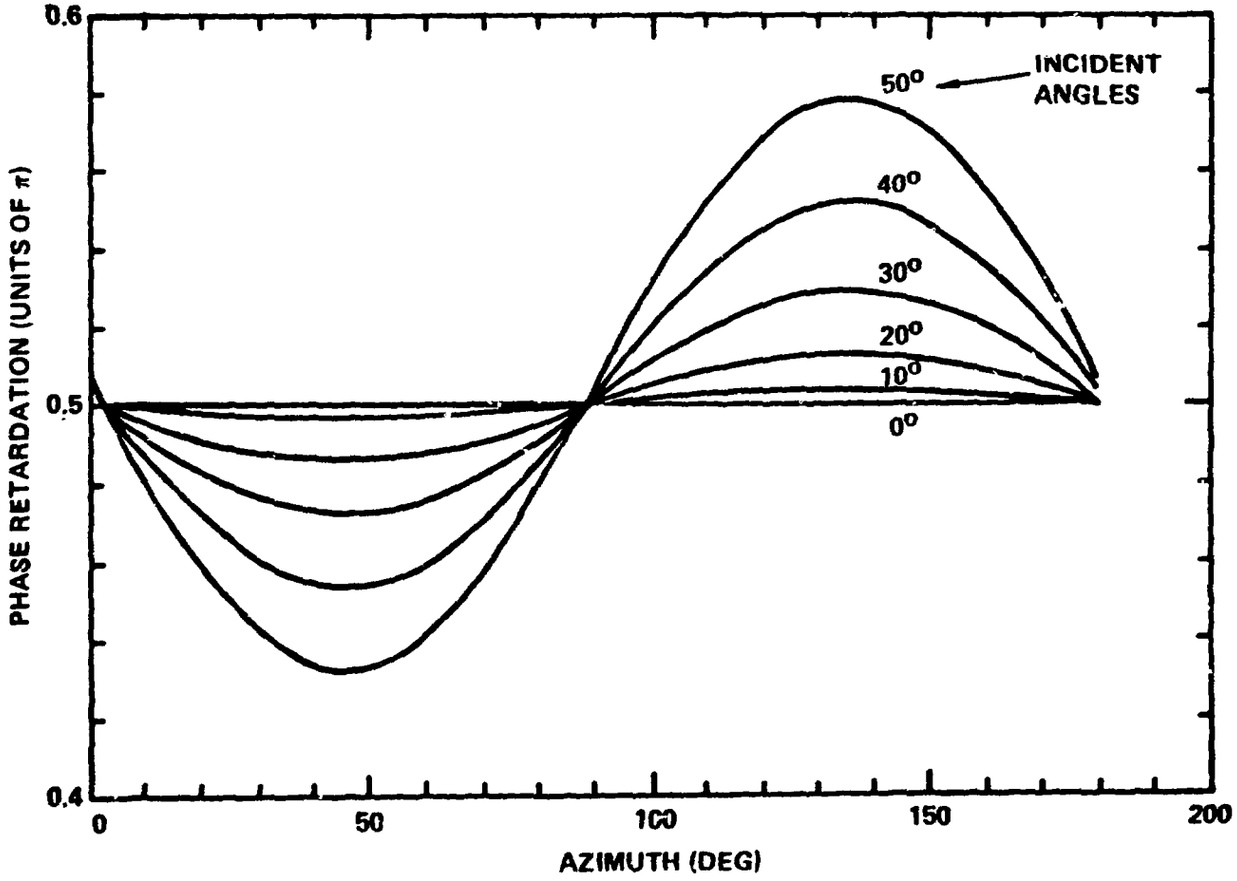


Fig. 21 Calculated phase retardation vs angle of incidence for a PVA half-waveplate. Phase retardation is plotted in units of full waves of retardation.

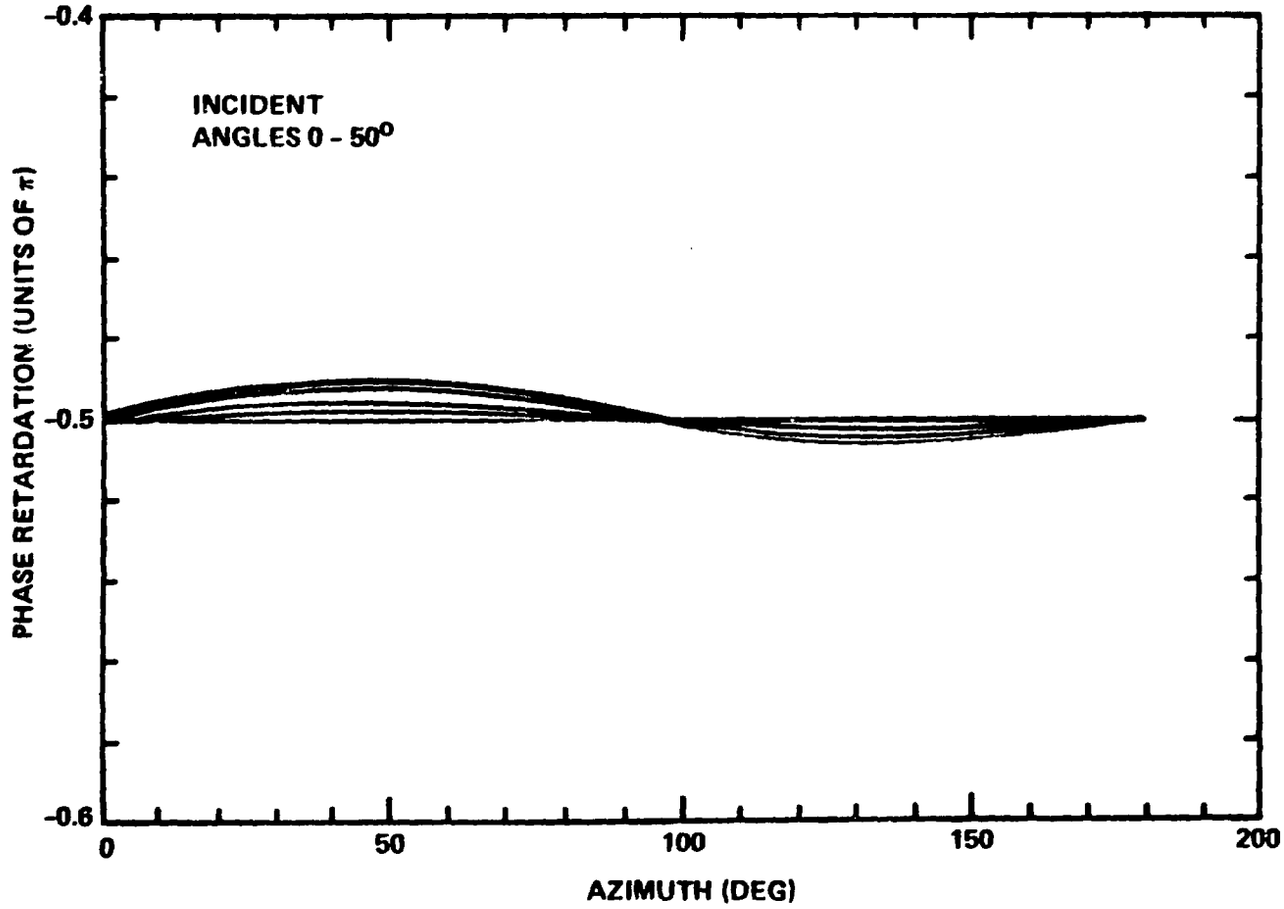


Fig. 22 Calculated phase retardation for a PVA-sapphire wide-field half-waveplate.

## 3.7 Filter Transmission

A wide variety of factors affect the peak transmission of the Lyot-type DBF. The principle loss contributions are: (1) polarizer losses, (2) birefringent material absorption, (3) Fresnel losses, and (4) scattering losses. Scattering losses are reducible by proper optical fabrication, and Fresnel losses between the various components are reduced by suitable anti-reflection coatings. The other losses are of more concern, and must be considered in the design of a DBF for any specific application. Polarizers represent a major loss mechanism. As a polarization device, a 50% insertion loss is experienced at the entrance polarizer. Subsequently, each polarizer absorbs some of the transmitted beam. HN-38 polarizer has an external transmission of only 76% for the transmitted component. Appropriate treatment of this material has been reported to increase the internal transmission to 95%.[38] In one laboratory test, we have achieved 90% internal transmission via heat treatment, and further improvements are expected. To illustrate the effect of polarizer absorption, Fig. 23 shows the maximum achievable transmission of a birefringent filter for different numbers of polarizers and values of polarizer transmission. In this calculation the effect of the 50% polarizer insertion loss has been included. Bulk absorption in the CdS is not included here. Summarizing projected polarizer losses for our present 7-stage filter, the polarizer limited transmission is expected to be $0.5 \times (0.95)^8 = 33\%$.

Since the present filter is designed for $\lambda = 5320$ Å, which is near the absorption edge, bulk absorption plays an important role. Using published values for the CdS absorption coefficients,[28] we predict 67% transmission from the total CdS thickness of 4.5 mm. Absorption measurements on CdS plates indicate increased absorption for some of the elements. This may be the result of incomplete sulfur annealing of the CdS material, or surface damage resulting from the optical fabrication,[28] and study of this issue is continuing.

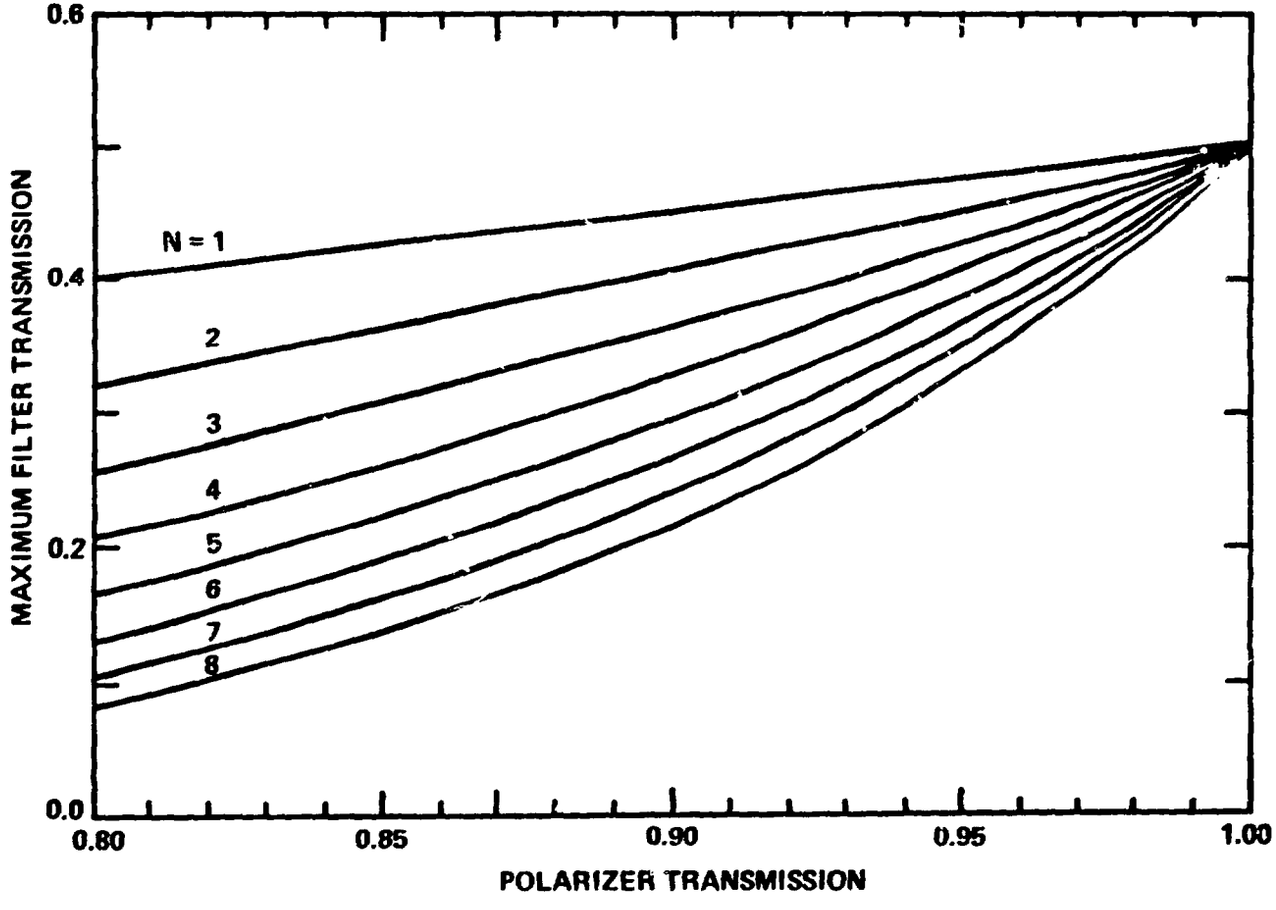


Fig. 23 Maximum potential filter transmission as a function of polarizer transmission and number of polarizers. 50% polarizer insertion loss has been included.

Summarizing these results, the predicted transmission of the 7-stage filter, at $\lambda$ = 5320 A, is 22%. Our present filter falls short of this as the result of Fresnel losses, low transmission polarizers, and increased absorption in several CdS plates, but at this writing, all of the contributions to transmission loss appear to be amenable to solution.

# 4.0 FUTURE DEVELOPMENTS

## 4.1 Materials

Thus far, our discussion has concentrated on DBF's fabricated using CdS. While this approach has been quite fruitful, future improvements in DBF's depend crucially on the identification and development of alternate material systems. Referring to Fig. 2 we see that at room temperature the region of strong dispersion in the birefringence of CdS extends from the iso-index wavelength out to at least 5550 A. However, the range over which it is practical to construct a DBF is somewhat narrower. On the short wavelength side, the bulk absorption of the CdS results in unsatisfactory filter transmission, while on the long wavelength end, the crystal plates required for a particular bandwidth become thicker as the dispersion decreases. Consequently, narrowband, room temperature CdS dispersive birefringence filters are practical in the wavelength range of 5300 A to 5400 A. Indeed, as discussed earlier, the bulk absorption of the CdS leads to significant loss even at 5320 A. It is clear that extension of DBF's to other wavelengths, as well as improvement in filter transmission, requires the use of alternate materials. To some extent, the useful range of CdS can be extended to shorter wavelengths by operating at reduced temperature. However, an analysis of the low temperature data is not yet complete.

One approach to the issue of alternate materials is to use mixed crystals. Laurenti, et al[39,40] have shown that the iso-index wavelength, and the region of large birefringence dispersion, can be greatly shifted to shorter wavelengths by substituting some zinc for cadmium in CdS and to longer wavelengths by substituting selenium for sulfur. Figure 24 illustrates the reported shift of iso-index point for various compositions of $Zn_xCd_{1-x}S$ and $CdS_{1-x}Se_x$ at 77k.

We have obtained a sample of graded composition $Zn_xCd_{1-x}S$, for evaluation, from Karlsruhe University. Measurements were made in two regions of the crystal which produced interference fringes of high visibility and

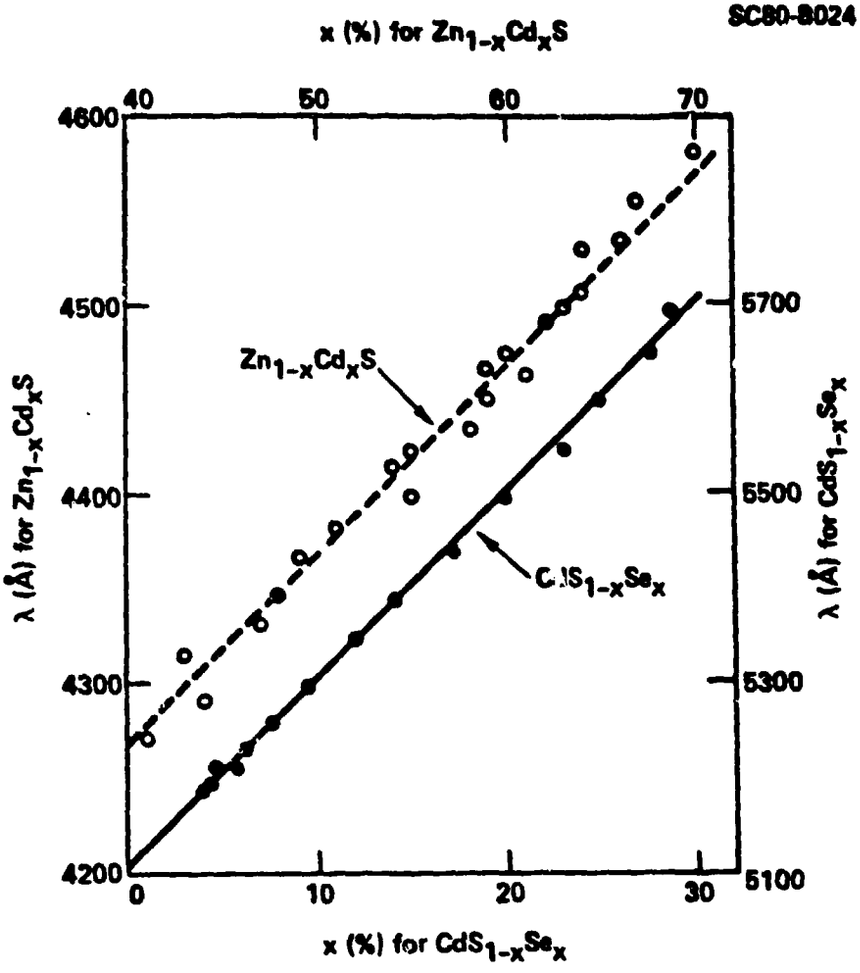


Fig. 24 Wavelength dependence of $\lambda_{ISO-INDEX_{40}}$ for $Zn_xCd_{1-x}S$ and $CdS_{1-x}Se_x$ at 77K. Reference Laurenti, et al.[40].

clear determination of the isotropic wavelength. One region, in the CdS rich end of the crystal, yielded results nearly identical to pure CdS ($\lambda_{iso\text{-}index}$ = 5230 A). The shift of the isotropic point from that of pure CdS was only 11 A. In the other clear region of the crystal, the iso-index point was shifted to $\lambda$ = 4846 A. Birefringence interference fringes were measured from the isotropic point, where the absorption was quite large, to 5080 A. The birefringence and its dispersion were determined, and are illustrated in Figs. 25 and 26. Chemical analysis of this sample indicated a zinc concentration of 14%.

If the results on the $Zn_{0.14}Cd_{0.86}S$ sample are compared with pure CdS, it is seen that the region over which high dispersion is observed is shifted by 400 A making shorter wavelength filters feasible. In fact, at a given distance from the isotropic point, the dispersion is greater for the $Zn_{0.14}Cd_{0.86}S$ which is a surprising result. Pure ZnS, in the wurtzite phase, has not been observed to have an isotropic point, and has minimal birefringence dispersion in its transparent region.[42] Since the bandedge and isotropic points vary monotonically as the zinc concentration increases, the increase of $d\Gamma/d\lambda$ for the measured concentration is difficult to understand. A thorough analysis of the band structure of this system will probably be required to explain this result. Efforts are presently underway to grow crystals of $Zn_xCd_{1-x}S$ of uniform composition.

Samples of $CdS_{1-x}Se_x$[23,24,40] are also being studied for longer wavelength applications. Initial results indicate a decrease in dispersion at room temperature, but low temperature results appear promising.

Other materials which may be of use for visible DBF's are $AgGaS_2$[43,44] and $CdGaS_4$.[45] In the ultra violet $Al_2O_3$ and $MgF_2$[25] have been observed to have a large dispersion in the birefringence, and $CdSe_{1-x}Te_x$[46] alloys may extend the range into the near infrared.

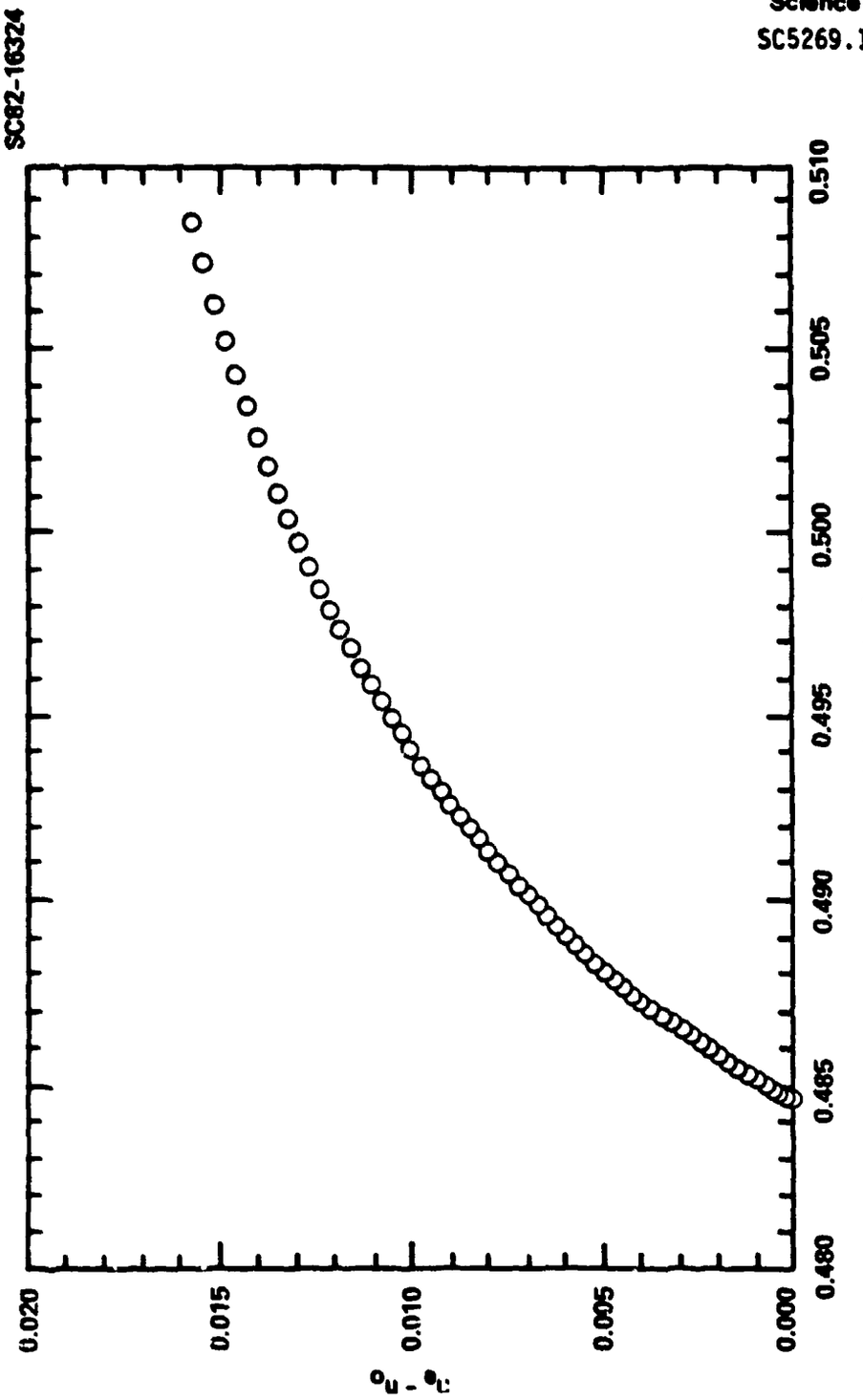


Fig. 25 Measured birefringence of $Zn_{0.14}Cd_{0.86}S$ at 300K.

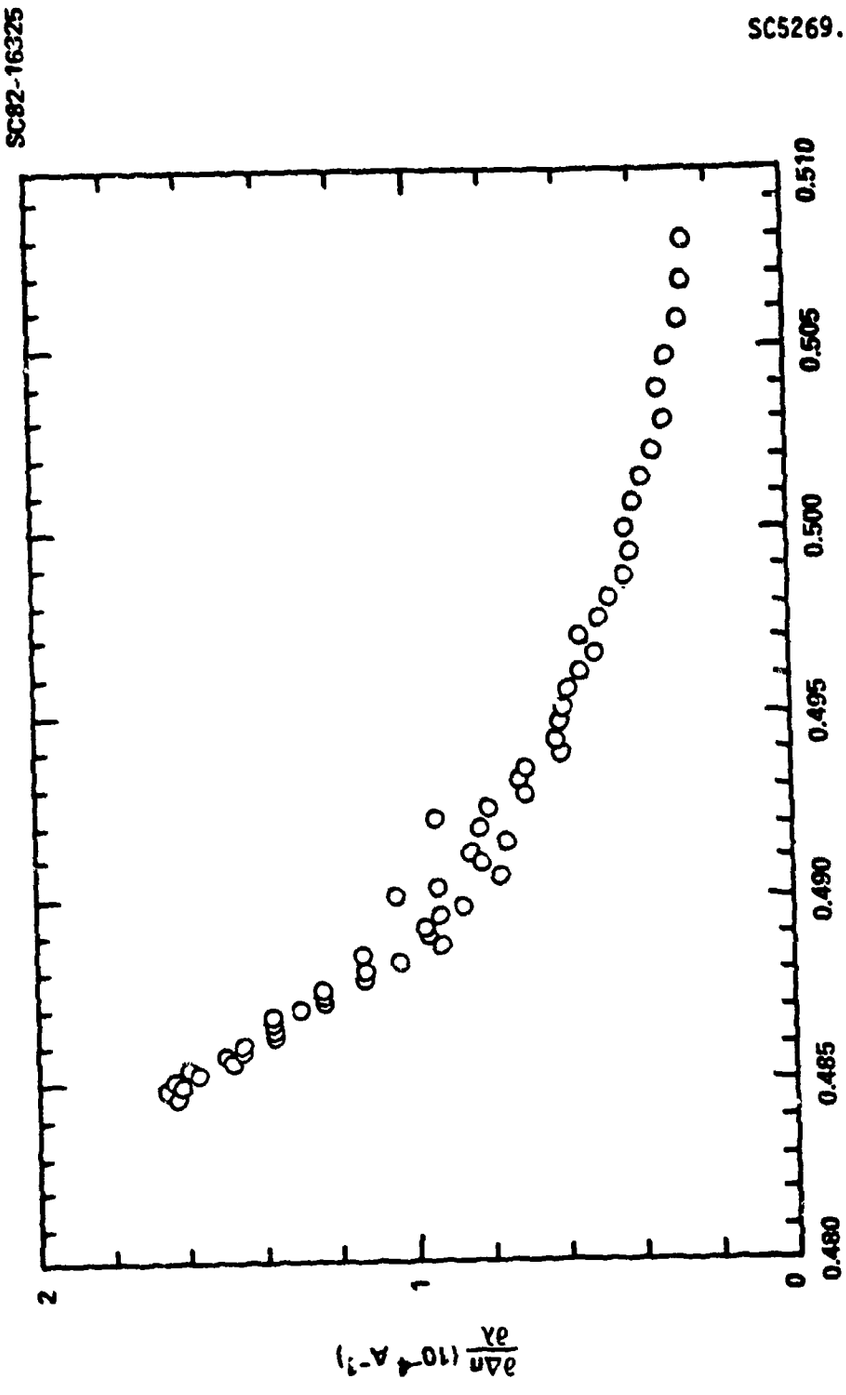


Fig. 26 Birefringence dispersion of $Zn_{0.14}Cd_{0.86}S$ at 300K.

## 4.2 Alternate Filter Configurations

At this stage of DBF development, the only filter configuration actively pursued has been the Lyot-type of structure. This design makes the most efficient use of birefringence material for a given bandwidth, and has ample polarizers to retain good out-of-band rejection at wide fields-of-view. However, the large number of polarizers required in a filter having a large FSR is beyond that required for wide-field operation, and presents a substantial loss in transmission. For this reason, alternate filter designs are desirable.

Solc filters,[20-22] and other related structures,[15,16] require fewer polarizers but very large numbers of low order elements. The FSR is largely determined by the thicknesses of the plates, while the bandwidth depends on their quantity. In a CdS filter, the first or second-order plates, required for adequate FSR, are three and six mils thick respectively, and would most likely require support. The many plates required for a narrowband filter would then lead to a thick structure, and vignetting losses would limit the FOV. In addition, Solc filters are much more sensitive to alignment errors than Lyot filters. Therefore, because of the difficulties anticipated in the fabrication of large numbers of thin plates, and the above stated considerations, simple Solc filters would probably not be feasible DBF structures.

A Solc-Lyot hybrid structure described by Title and Rosenberg,[47] may be a promising approach. Figure 27 shows a schematic of a single stage of this filter. This design boasts very low out-of-band transmission, and each stage has a relatively large FSR for the number of plates required. Calculations have shown that this filter, using a single hybrid stage of CdS in tandem with two or three simple Lyot-Öhman low order stages, can completely eliminate sidebands in the visible, and still result in a narrow passband. Fewer polarizers are required than for a traditional Lyot-Öhman filter, and fewer thin plates are required than for a simple Solc filter.

Other modifications of the device structure will undoubtedly be realized and implemented as DBF technology matures.

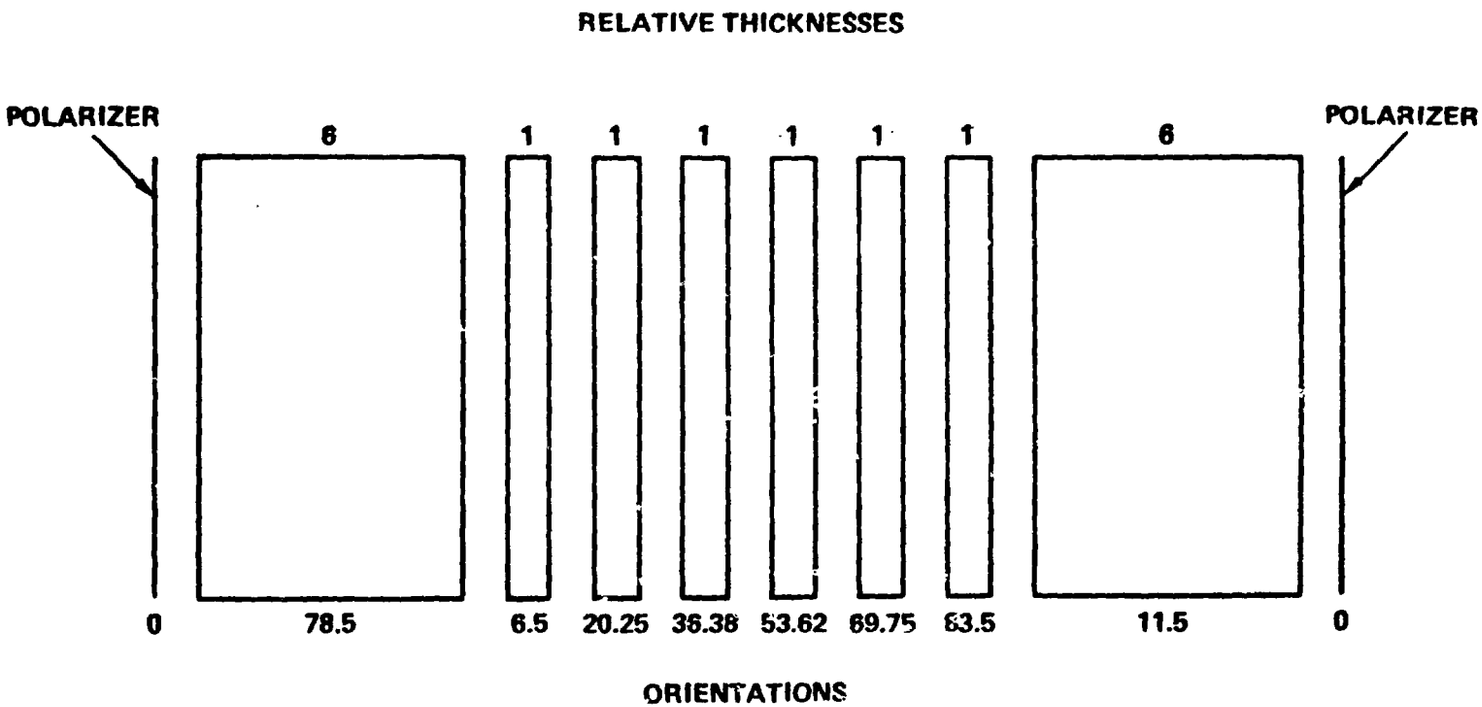


Fig. 27 Single stage Solc-Lyot hybrid structure. Reference Rosenberg and Title[47].

## 5.0 REFERENCES

1. S. Karp, "Optical Communications Between Underwater and Above Surface (Satellite) Terminals," IEEE Trans. Comm. COM-24, 66-81 (1976).

2. G.C. Mooradian, "Surface and Subsurface Optical Communications in the Marine Environment," Opt. Eng. 20, 71 (1981).

3. J.H. Shapiro and C. Warde, "Optical Communication Through Low-Visibility Weather," Opt. Eng. 20, 76 (1981).

4. A.M. Title and W.J. Rosenberg, "Improvements in Birefringent Filters 5: Field-of-View Effects," Appl. Opt. 18, 3443 (1979).

5. R.M. Lerner, "Limitations in the Use of Dielectric Interference Filters in Wide Angle Optical Receivers," Appl. Opt. 10, 1914 (1971).

6. J.B. Marling, J. Nilson, L.C. West, and L.L. Wood, "An Ultrahigh-Q Isotropically Sensitive Optical Filter Employing Atomic Resonance Transitions," J. Appl. Phys. 50, 610 (1979).

7. J.F. Lotspeich, "Iso-index Coupled-Wave Electro-Optic Filter," IEEE J. Quantum Electron. QE-15, 904 (1979).

8. P. Yeh, "Dispersive Birefringent Filters," Opt. Commun. 37, 153 (1981).

9. P. Yeh and J. Tracy, "Theory of Dispersive Birefringent Filters," Proc. SPIE, 268, 171 (1981).

10. W. Gunning, R. Hall, P. Yeh, and J. Tracy, "Dispersive Birefringent Filters; Experimental Development," submitted to Appl. Optics.

11. P. Yeh, W. Gunning, R. Hall, and J. Tracy, "Dispersive Birefringent Filters for Laser Communications," presented at the Conference of Lasers and Electro-Optics, Washington, D.C., June 10-12 (1981).

12. W. Gunning, R. Hall, P. Yeh, and J. Tracy, "Dispersive Birefringent Filters for Blue-Green Communications," presented at the 1981 OSA Annual Meeting, October 27-30, Kissimee, Florida.

13. H. Gobrecht and A. Bartschat, "On the Birefringence of Cadmium Sulfide," Z. fur Physik, 156, 131 (1959).

14. S.A. Abagyan, G.A. Ivanov, Yu.A. Lamov, and Yu.E. Shanurin," Spectral Dependence of the Birefringence of CdS," Sov. Phys. Semicond. 4, 2049 (1971).

15. S.E. Harris, E.O. Ammann, and I.C. Chang, "Optical Network Synthesis Using Birefringent Crystals. I. Synthesis of Lossless Networks of Equal Length Crystals," J. Opt. Soc. Am. 54, 1267 (1964).

16. A.M. Title and W.J. Rosenberg, "Spectral Management," Proc. SPIE 268, 178 (1980).

17. B. Lyot, "The Birefringent Filter and its Applications in Solar Physics," Ann. Astrophys. 7, 31-79 (1944).

18. Y. Öhman, "A New Monochromator," Nature 141, 157 (1938); "A New Mochromator," Nature 141, 291 (1938).

19. J.W. Evans, "The Birefringent Filter," J. Opt. Soc. Am. 39, 229 (1949); "The Birefringent Filter: A Correction," J. Opt. Soc. Am. 39, 412 (1949).

20. I. Solc, "A New Type of Birefrigent Filter," Czech. J. Phys. 4, 53 (1954).

21. I. Solc, "Birefringent Chain Filters," J. Opt. Soc. Am. 55, 621 (1965).

22. J.W. Evans, "Solc Birefringent Filters," J. Opt. Soc. Am. 48, 142 (1958).

23. A.A. Reza, G.A. Babonas, and A.Yu. Shileika, "Dispersion of the Temperature Coefficients of the Birefringence of CdS and CdSe," Sov. Phys. Semicond. 9, 986 (1976).

24. M.P. Lisitsa, L.F. Gudymenko, V.N. Malinko, and S.F. Terekhova, "Dispersion of the Refractive Indices and Birefringence of $CdS_xSe_{1-x}$ Single Crystals," Phys. Stat. Sol. 31, 389 (1969).

25. V. Chandrasekharan and H. Damany, "Anomalous Dispersion of Birefringence of Sapphire and Magnesium Fluoride in the Vacuum Ultraviolet," Appl. Opt. 8, 671 (1969).

26. J.M. Beckers, "Achromatic Linear Retarders," Appl. Opt. 10, 973 (1971).

27. A.M. Title, "Effective Index of Calcite and Quartz," Sol. Phys. 39, 505 (1974).

28. D.G. Thomas, J.J. Hopfield, and M. Power, "Excitons and Absorption Edge of Cadmium Sulfide," Phys. Rev. 119, 570 (1960).

29. See for example D.G Thomas, ed. II-VI Semiconducting Compounds 1967 International Conference, W.A. Benjamin, New York, Amsterdam (1967).

30. D. Dutton, "Fundamental Absorption Edge in Cadmium Sulfide," Phys. Rev. 112, 785 (1958).

31. E. Gross, S. Permogorov, V. Travnikov, and A. Selkin, "Hot Excitons and Exciton Excitation Spectra," J. Phys. Chem. Solids 31, 2595 (1970).

32. D.G. Thomas and J.J. Hopfield, "Exciton Spectrum of Cadmium Sulfide," Phys. Rev. 116, 573 (1959).

33. C.H. Henry, "Coupling of Electromagnetic Waves in CdS," Phys. Rev. 143, 627 (1966).

34. T.M. Bieniewski and S.J. Czyzak, "Refractive Indices of Single Hexagonal ZnS and CdS Crystals," J. Opt. Soc. Am. 53, 496 (1963).

35. P. Roche, L. Bertrand, and E. Pelletier, "Influence of Temperature on the Optical Properties of Narrowband Interference Filters," Optica Acta 23, 433 (1976).

36. A.M. Title, "Improvement of Birefringent Filters. I. Reduction of Scatter in Polaroid Materials," Sol. Phys. 33, 521 (1973).

37. P. Yeh, Proc. SPIE 307, Paper No. 307-3 (1981); "Extended Jones Matrix Method," accepted for publication J. Opt. Soc. Am.

38. A. Title and W. Rosenberg, "Research on Spectroscopic Imaging," NASA Final Report NASW-3107, pp. 61-64 (1979).

39. J.P. Laurenti, K.C. Rustagi, and M. Rouzeyre, "Optical Filters Using Coupled Light Waves in Mixed Crystals," Appl. Phys. Lett. 28, 212 (1976).

40. J.P. Laurenti, K.C. Rustagi, M. Rouzeyre, H. Rufer, and W. Ruppel, "Graded-Composition Semiconductors as Tunable Narrow-band Optical Filters," J. Appl. Phys. 48, 203 (1977).

41. W. Gunning, J. Tracy, and H. Rufer, "Birefringence of $Zn_xCd_{1-x}S$ Near the Isotropic Point," in preparation.

42. M. Cardona and G. Harbeke, "Optical Properties and Band Structure of Wurtzite-Type Crystals and Rutile," Phys. Rev. 137, A1467 (1965).

43. V.V. Badikov, I.N. Matveev, S.M. Pshenichnikov, O.V. Skrebneva, N.K. Trotsenko, and N.D. Ustinov, "Study of Dispersion of Birefringence and Optical Activity of Silver Gallium Sulfide Selenide ($AgGa(S_{1-x}Se_x)_2$) Crystals," Kristallografiya 26, 537 (1981).

44. G.D. Boyd, H. Kasper, and J.H. McFee, "Linear and Nonlinear Optical Properties of $AgGaS_2$, $CuGaS_2$, and $CuInS_2$, and the Theory of the Wedge Technique for the Measurement of Nonlinear Coefficients," IEEE J. Quantum Electron. QE-7, 563 (1971).

45. L.M. Suslikov, Z.P. Gadmashi, I.F. Kopinets, E.Yu. Peresh and V.Yu. Slivka, "Birefringence of $CdGa_2S_4$ Single Crystals," Opt. Spectrosc. 49, 51 (1981).

46. R.B. Parsons, W. Wardzynski, and A.D. Yoffe, "The Optical Properties of Single Crystals of Cadmium Selenide," Proc. Roy. Soc. London Ser. A 262, 120 (1961).

47. W.J. Rosenberg, and A.M. Title, "Solc Filter Engineering," Proc. SPIE, 307, pp. 307-21 (1981).